1 *In vitro* and *in vivo* analysis of microvesicle-mediated metastasis

2 using a bright, red-shifted bioluminescent reporter protein of

3 extracellular vesicles

4

5 Ahmed A. Zarea[*1], Gloria I. Perez[*1,2], David Broadbent[1,2], Benedikt Dolgikh[1,4], Matthew

6 P. Bernard[1,3], Alicia Withrow[8], Amelia McGill[1], Victoria Toomajian[1,5], Lukose K.

7 Thampy[1,2], Jack Harkema[3], Joel R. Walker[9], Thormas A. Kirkland[9], Michael H.

8 Bachmann[1,6], Jens Schmidt[1,7], and Masamitsu Kanada[**1,3]

9

10 **Affiliations**

11 [1]Institute for Quantitative Health Science and Engineering (IQ), [2]College of Osteopathic

12 Medicine, [3]Department of Pharmacology & Toxicology, [4]College of Natural Science,

13 [5]Department of Biomedical Engineering, [6]Department of Microbiology & Molecular

14 Genetics, [7]Department of Obstetrics and Gynecology, College of Human Medicine,

15 [8]Center for Advanced Microscopy, Michigan State University, East Lansing, Michigan.

16 [9]Promega Biosciences LLC, 227 Granada Dr, San Luis Obispo, CA.

17

18 *These authors contributed equally to this work.

19

20   **Corresponding author: Masamitsu Kanada, Michigan State University, 775 Woodlot Dr.

21   East Lansing, MI 48824. Phone: (517) 884-6933; Fax: (517) 884-7463; E-mail:

22   kanadama@msu.edu

23

24

25   **Abstract**

26   Cancer cells produce heterogeneous extracellular vesicles (EVs) as mediators of

27   intercellular communication. Our study focused on a novel method to image EV subtypes

28   and their biodistribution *in vivo*. Regardless of injection routes, we established that

29   reporter EVs isolated from murine mammary carcinoma cells expressing PalmReNL,

30   which utilizes bioluminescence resonance energy transfer (BRET), localized to the lungs.

31   This new EV reporter allowed highly sensitive EV tracking *in vitro* and *in vivo* and enabled

32   us to begin studies to understand the commonalities and functional differences of the EV

33   subtypes. We demonstrated the early appearance of metastatic foci in the lungs of

34   mammary tumor-bearing mice following multiple injections of the microvesicle (MV)-

35   enriched fraction derived from mammary carcinoma cells. In addition, the results we

36   present here show that tumor cell-derived MVs act on distant tissues through upregulating

37   LC3 expression within the lung.

38

39

Introduction

Extracellular vesicles (EVs) are spherical lipid bilayered structures naturally shed by cells and have been implicated in the pathogenesis of cancer and numerous other diseases[1,2]. Understanding their biodistribution and ultimate targets is key to elucidating their roles in health and disease[3,4]. EV subtypes include exosomes and microvesicles (MVs), which are distinguished based on their size and biogenesis[1,2]. Exosomes range from ~30-120 nm in diameter and are produced by inward budding of the late endosomal membrane, known as multivesicular bodies (MVBs). MVs are 50-1000 nm in diameter and produced by simple outward budding of the plasma membrane. Due to their nano-size and biophysical properties, both types of EVs have the potential to cross biological barriers and gain access into host cells beyond these barriers[5-7]. In this manner, released EVs act as mediators of intercellular communication in the body[8,9]. For example, numerous studies have demonstrated that cancer cells can appropriate this communication pathway by transferring active biomolecules to adjacent and distant cancer cells, promoting their growth and survival[2,10]. For this reason, EV-mediated signaling may hold promising cancer treatment strategies and be an effective platform for drug delivery. However, systemic administration of nano-sized EVs may reach and accumulate in other sites beyond the tissues of therapeutic interest[11-13]. Therefore, analysis of the biodistribution following EV administration is a prerequisite for the development of EV-based therapeutics.

Characterization of EV biodistribution, however, is restricted by the biological tools available, which are not sensitive enough to localize and track small EVs *in vivo*. In this study, we develop a novel EV reporter system that enables highly sensitive EV tracking.

63   Non-invasive *in vivo* bioluminescence imaging combined with molecular and cellular

64   analyses offers unique potential to facilitate the preclinical evaluation of biological

65   therapies in animal models. Additionally, most *in vivo* studies of EV-mediated signaling

66   have only used immune-compromised mice[3,14] and require further assessment in the

67   presence of an intact immune system. In our current studies, combining *in vitro* and *in*

68   *vivo* approaches with immunocompetent mice, we expect to uncover some of the

69   biological characteristics of EVs, such as trafficking, cellular uptake and release.

70

71   **Results**

72   **Overexpression of PalmReNL labeled both exosomes and MVs.**

73   We developed PalmReNL, a novel EV imaging probe, by genetically fusing a

74   palmitoylation signal peptide[15] to one of the brightest red-shifted bioluminescence

75   resonance energy transfer (BRET) reporters, Red-eNanoLantern (ReNL)[16] (Fig. 1a). We

76   observed that PalmReNL supplied with its substrate furimazine (Fz) produced red-shifted

77   luminescence similar to that of ReNL without palmitoylation, indicating that membrane-

78   anchoring of ReNL does not affect its BRET efficiency (Fig. 1b). This EV reporter has an

79   advantage for *in vivo* tracking since bioluminescence imaging produces negligible

80   background signals. Also, photons with spectral wavelengths longer than 600 nm can

81   efficiently penetrate mammalian tissues with less light attenuation than observed with

82   shorter wavelength light. Moreover, PalmReNL can be used as a fluorescent EV reporter

83   by exciting tdTomato for standard flow cytometry and microscope settings.

84   As reported previously[15], the results of the experiments to determine the membrane

85   orientation of PalmReNL in EVs, revealed that PalmReNL can label the inner membrane

86   leaflet of both exosomes and MVs. However, there were differences in the outer

87   membrane labeling by PalmReNL between exosome- and MV-enriched fractions. As

88   demonstrated by both the dot blot (Supplementary Fig. 1f-i) and the proteinase-K

89   protection assays (Fig. 1c, d), in exosomes the reporter was protected from Proteinase-

90   K, hence localized primarily to the inner membrane. In contrast, in MVs PalmReNL was

91   sensitive to Proteinase-K without detergent treatment, indicating that it localized to both

92   the inner and the outer membranes. This dual-labeling of exosomes and MVs represents

93   an advantage over other widely used CD63-based EV reporters that only label one

94   specific EV subtype, exosomes[17].

95   We next assessed the labeling efficiency in isolated exosome- and MV-enriched fractions

96   from 4T1 cells stably expressing PalmReNL. Firstly, exosomes and MVs were isolated

97   from the conditioned medium as we previously reported[18,19] and characterized by

98   nanoparticle tracking analysis (NTA). The concentration of MVs expressing PalmReNL

99   was 7.7×10^{10} particles/mL and the mean diameter was 119 nm (Supplementary Fig. 1b),

100   while the concentration of exosomes expressing PalmReNL was 1.9×10^{10} particles/mL

101   and the mean diameter was 105 nm (Supplementary Fig. 1a). The concentrations and

102   mean diameters of exosome- and MV-enriched fractions derived from control 4T1 cells

103   were 1.9×10^{10} particles/mL and 102 nm, 2.7×10^{10} particles/mL and 117 nm,

104   respectively (Supplementary Fig. 1c, d). Therefore, the genetic addition of the reporter

105   did not inhibit the release of EVs nor influence their sizes. Determination of the Zeta

106   potential revealed that the PalmReNL slightly shifted the surface charge of exosomes,

107   but not MVs (Supplementary Fig. 1e). Consistent with the NTA data, the transmission

108   electron microscopy (TEM) analysis of the exosome- and MV-enriched fractions revealed

109   a heterogeneous mixture of predominantly intact vesicles with artefactual cup-shaped

110   morphology[20] having diameters ranging from 50 to 200 nm, and expressing the tdTomato

111   as ReNL is a fusion protein of NanoLuc and tdTomato[16] (Fig. 1h, i). There was no

112   significant morphological change in the EV fractions expressing PalmReNL.

113   Western blot (WB) analysis of exosome marker proteins in immunoblots of whole-cell

114   lysates and EVs derived from 4T1 cells expressing PalmReNL (Supplementary Fig. 1k)

115   demonstrated that exosome fractions preferentially express CD63, TSG101, and Alix,

116   whereas cell lysates and MV-enriched fractions preferentially express Flotillin-1 as we

117   previously reported[19]. Importantly, WB analysis of EVs collected from the parental 4T1

118   cell line demonstrated that the reporter protein (PalmReNL) does not interfere with the

119   expression of any of the EVs marker proteins tested (Supplementary Fig. 1j). All fractions

120   of EVs containing PalmReNL (cell lysates, MVs, and exosomes) expressed tdTomato.

121   The labeling efficiency was also confirmed by fluorescence microscopy, demonstrating

122   that the total fluorescence intensities were higher in exosomes, but punctate signal

123   intensity was higher for individual MVs (Fig. 1e-g). To further assess the efficiency of EV

124   labeling with PalmReNL, we analyzed individual PalmReNL-exosomes and -MVs by flow

125   cytometry (Fig. 1j, k). Firstly, all the isolated PalmReNL-EVs were stained with CellTrace

126   Violet (CTV) as an alternative to CFSE, an amine-reactive dye previously used for

127   nanoFACS[21]. The PalmReNL signal was detected on the tdTomato channel, and the

128   percentage of positive labeling was 1.2% for exosomes and 6.3% for MVs stained with

129   CTV (Fig. 1l). The median fluorescence intensity (MFI) of PalmReNL in individual MVs

130 was 1.27-fold higher than that of exosomes (Fig. 1m). As we previously reported,

131 phosphatidylserine (PS) externalization in exosomes and MVs was examined using

132 Annexin V staining[18]. The fluorescence signals in individual exosomes were significantly

133 higher than the signals in individual MVs, where 95.4% and 52.9% of PS externalization

134 was detected in exosomes and MVs stained with CTV, respectively (Fig. 1l). The MFI of

135 Annexin V in individual MVs was 2.6-fold lower than that of exosomes among the CTV-

136 stained EVs (Fig. 1m).

137 Furthermore, we found that the release of EVs from 4T1 cells-expressing PalmReNL *in*

138 *vitro* occurs every 24 h and peaks at 72 h. The bioluminescence signals in both

139 exosomes- and MVs-PalmReNL correlated with the number of particles present, and

140 increased steadily over the 72 h period (Supplementary Fig. 2b, c). The reporter 4T1 cells

141 appear to release ~20-fold more MVs than exosomes as assessed by NTA. The

142 bioluminescence signals were also correlated with the number of EVs purified from

143 different EV fractions after density gradient ultracentrifugation (Supplementary Fig. 2d).

144 Measuring the bioluminescence signals in equal numbers of PalmReNL-exosomes and -

145 MVs ranging from 2.5×10^6 to 1.0×10^7 using 25 µM Fz demonstrated that the

146 bioluminescence signals in the exosomes ($1.9 \times 10^5 \pm 1.4 \times 10^4$ RLU; $p<0.0001$) were 1.7-

147 fold higher than those of the MVs ($1.1 \times 10^5 \pm 1.8 \times 10^3$ RLU). A novel Fz analogue, named

148 fluorofurimazine (FFz), with increased aqueous solubility was recently developed[22]. We

149 found FFz was 1.4- and 1.5-fold more sensitive (exosomes $2.6 \times 10^5 \pm 3.9 \times 10^3$ RLU,

150 $p=0.0012$; MVs $1.7 \times 10^5 \pm 3 \times 10^3$ RLU, $p<0.0001$) than Fz (Fig. 1n) with PalmReNL-

151 exosomes and -MVs, respectively. The protein concentrations of 5.6×10^7 EV particles

152 were 45.4 µg/mL for exosomes and 23.9 µg/mL for MVs. Furthermore, the

153   bioluminescence spectra of PalmReNL-exosomes and -MVs were measured with similar

154   emission spectra, peaking at 585 nm (Fig. 1o). Taken together, these results suggest that

155   exosomes incorporate PalmReNL more efficiently compared to MVs. However,

156   fluorescence signals in individual exosomes are below the detection limit and only

157   individual MVs carry fluorescently detectable numbers of PalmReNL molecules due to

158   the larger surface areas relative to exosomes and/or symmetrical labeling of MV

159   membranes.
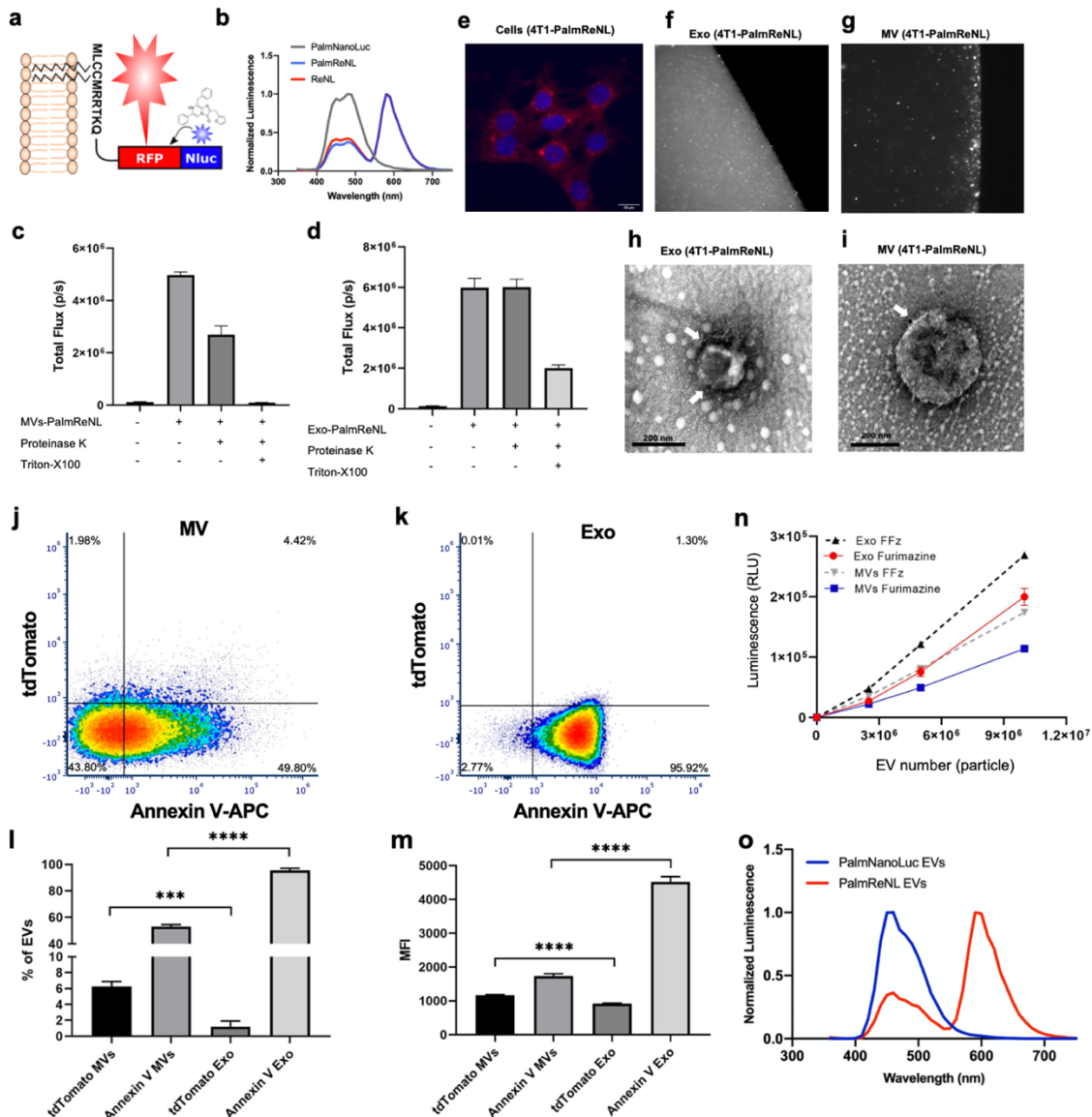
160

Fig. 1 PalmReNL-based labeling of exosomes and MVs derived from 4T1 cells. a Schematic diagram of EV membrane labeling with PalmReNL BRET probe. **b** Emission spectra of murine mammary carcinoma 4T1 cells transfected with ReNL, PalmReNL, or PalmNanoLuc. **c, d** Proteinase-K protection assay for PalmReNL-MVs and exosomes. **e** 4T1 cells constitutively expressing PalmReNL. Punctate signals of RFP (red) were merged with nuclei stained with Hoechst 33342. Scale bar, 20 μm. **f, g** A droplet of buffer containing isolated PalmReNL-exosomes and -MVs. **h, i** Transmission electron microscopy of 4T1 cell-derived PalmReNL-exosomes or -MVs, immunogold labeled for RFP. Arrows point towards positive RFP signal (dark spots). Scale bars, 200 nm. **j, k** A representative of three independent experiments of Annexin V staining of individual PalmReNL-MVs and -exosomes analyzed by flow cytometry. The tdTomato fluorescence signal represents PalmReNL-EVs. FACS plots were gated for tdTomato$^+$ and Annexin V$^+$ EVs among the CTV-stained EVs. **l, m** The percentage and median fluorescence intensity (MFI) of positively labeled CTV-exosomes and -MVs. Error bars, SD (n = 3), ***, P < 0.001; ****, P < 0.0001. **n** Bioluminescence analysis of PalmReNL-exosomes and MVs using furimazine and fluorofurimazine (FFz). Error bars, SD (n = 5). **o** Emission spectra of the isolated PalmNanoLuc- and PalmReNL-EVs**.**

161

Rates of endocytosis of tumor cell-derived exosomes and MVs were similar between various recipient cell types.

Uptake of PalmReNL-exosomes and MVs by macrophages (Fig. 2a-c), 4T1 cells (Fig. 2d-f), lung fibroblasts (Fig. 2g-i), or adipose-derived mesenchymal stromal cells (AMSCs) were assessed (Fig. 2j-l). Phase contrast and fluorescence microscopy demonstrated that EV-uptake was time-dependent. In our experimental conditions the 24 h time point showed the highest fluorescence. Of note, the fluorescence signals of our reporter EVs decreases over time, which is an advantage compared to the widely used lipophilic fluorescent dyes such as PKH, DiR, and DiI which can persist in the recipient cells. These dyes previously showed inaccurate spatiotemporal information on the reporter EVs due to its inherent stability[15,18].

173   The bioluminescence signal did not reveal any significant differences between the cell

174   types in the uptake of the reporter, except at 2 h between RAW 264.7 cells and lung

175   fibroblasts where the bioluminescence signal of PalmReNL-MVs was significantly higher

176   $(3.1 \times 10^8 \pm 2.5 \times 10^7$ and $2.2 \times 10^8 \pm 7.1 \times 10^6$ p/s, respectively; p=0.004). Both cell types

177   had a significantly lower (p<0.05) bioluminescence signal of PalmReNL-MVs at 24 h

178   (Supplementary Fig. 3a-d). By contrast, the uptake of PalmReNL-exosomes appeared to

179   remain constant during the 24 h period in all cell types tested. Next, we assessed the

180   mechanism of cellular uptake of exosomes and MVs. Inhibition of caveolin-dependent

181   endocytosis, which was inhibited by methyl-β-cyclodextrin (MβCD; a compound that

182   sequesters the cholesterol in the cell membrane[23]), significantly decreased the MV-

183   uptake in all cell types studied (Fig. 2m-p). Interestingly, MV uptake in Raw 264.7 cells

184   appears to occur by both clathrin-dependent endocytosis inhibited by chlorpromazine[24]

185   and caveolin-dependent endocytosis (Fig. 2m, q). On the other hand, the uptake of

186   exosomes in all the cell types tested was independent of both caveolin and clathrin (Fig.

187   2m-t).
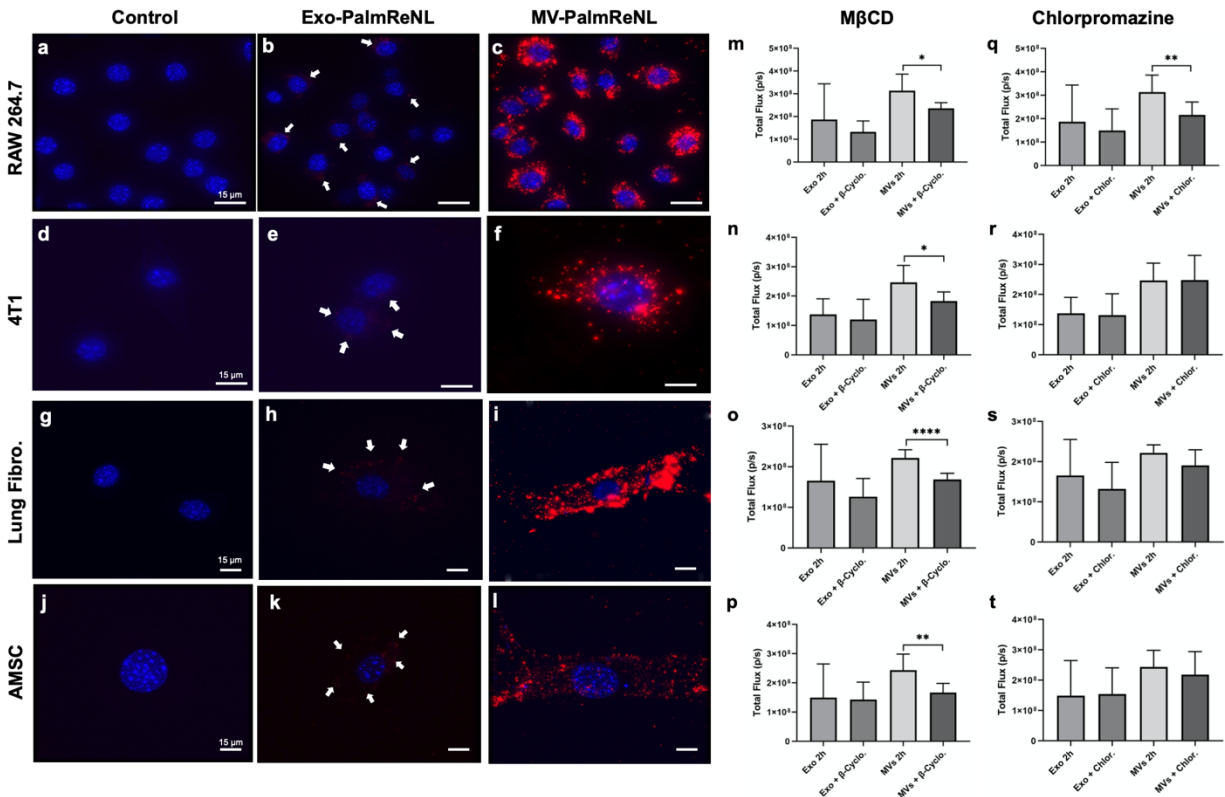
188

Fig. 2 Similar rates of endocytosis of 4T1 cell-derived exosomes- and MVs-PalmReNL between various recipient cell types *in vitro*. a-c Macrophages (RAW 264.7). **d-f** 4T1 cells. **g-i** primary mouse lung fibroblasts. **j-l** Adipose-derived mesenchymal stromal cells (AMSCs). Punctate signals of RFP (red) were merged with nuclei stained with Hoechst 33342 (blue). Scale bar, 15 μm. Arrows indicate weak RFP signals in PalmReNL-exosomes. **m-t,** The recipient cells were treated with methyl-β-cyclodextrin (MβCD; 10 mM) (m-p) or Chlorpromazine (10 ug/mL) (q-t). **m, q** Macrophage RAW 264.7 cells. **n, r** 4T1 cells. **o, s** Mouse primary lung fibroblasts. **p, t** Mouse AMSCs. Error bars, SD (n = 8), *, P < 0.05; **, P < 0.01; ****, P < 0.0001.

189   Although the bioluminescence signal for PalmReNL-exosomes was higher than that of

190   MVs-PalmReNL (see Fig. 1n), detecting exosome uptake by fluorescence microscopy

191   was challenging. We hypothesized that our inability to detect the PalmReNL-exosomes

192   reflects those reporter exosomes cannot retain the fluorescence signal after being taken

193   up by the cells. Rapid diffusion of the PalmReNL into other cellular membrane

194   compartments might result in a fast loss of signals. To prove this, we compared the *in*

195   *vitro* uptake by RAW 264.7 macrophages or 4T1 cells of exosomes derived from 4T1 cells

11

196 stably expressing the exosome marker CD63 fused with mScarlet[25] or PalmReNL. CD63-

197 mScarlet-exosomes showed punctate fluorescence signals in both recipient 4T1 and

198 RAW 264.7 cells (Fig. 3c, f), demonstrating their cellular uptake and signal retention after

199 being taken up by cells. On the other hand, PalmReNL-exosomes did not retain the

200 signals after being taken up by cells and therefore precluded their visualization with the

201 current sensitivity and resolution of our microscope (Fig. 3b, e). However, exosomes

202 carrying PalmReNL retained bioluminescence in the recipient cells (see Supplementary

203 Fig. 3). These results indicate that PalmReNL carried by exosomes might be rapidly

204 transfered from early endosomes into other membrane compartments for either

205 degradation or recycling, whereas transferred CD63-mScarlet may be retained in

206 endosomal membranes in recipient cells as recently reported[17].

207 To further assess the effect of acidic cellular compartments on PalmReNL-exosomes, we

208 used Palm-fused Gamillus (acid-tolerant monomeric GFP[26]) for EV labeling and

209 compared the uptake of exosomes by fluorescence microscopy. At 24 h the exosomes-

210 PalmGamillus signal was easily detected by fluorescence microscopy compared to the

211 PalmReNL-exosomes signal which was barely detected (Supplementary Fig. 4b, c).

212 Moreover, treatment of cells with inhibitors of endosomal acidification, either

213 Concanamycin A[27] or Chloroquine[28] significantly increased the bioluminescence signal of

214 PalmReNL-exosomes (Fig. 3g). Since the loss of NanoLuc activity with endosomal

215 translocaiton was previously reported[29], we analyzed the pH sensitivity of EVs-

216 PalmReNL. The bioluminescence signals of both PalmReNL-exosomes and -MVs

217 steadily decreased at pH below 6.0 either with or without detergent treatment (Fig. 3h, i),

218 indicating significant signal loss of PalmReNL-based EV reporters in acidic cellular

219 compartments.
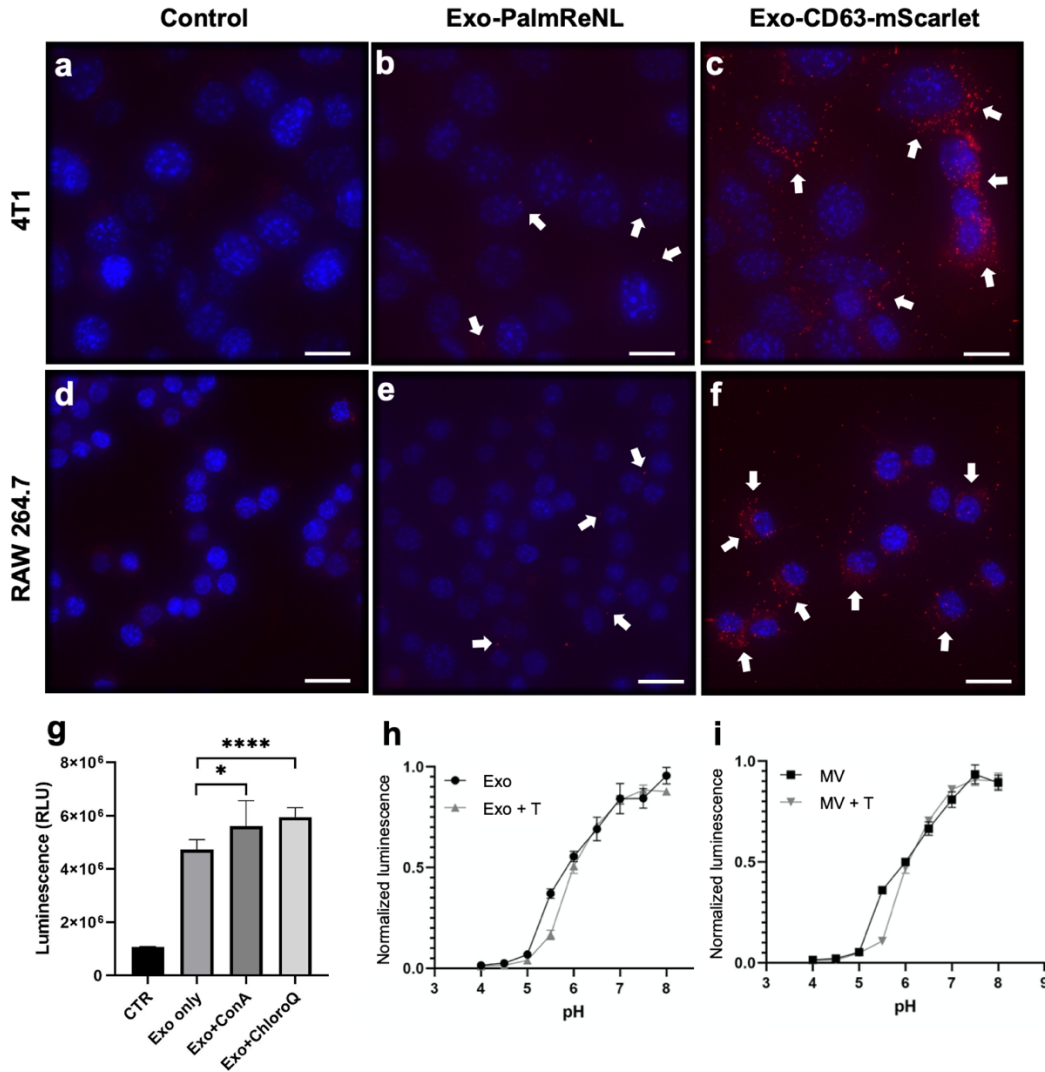
220

Fig. 3 Rapid processing of PalmReNL carried by exosomes via the endosomal-lysosomal pathway. Fluorescence microscopy images of 4T1 and RAW 264.7 cells treated for 24 h with PalmReNL- or CD63-mScarlet-exosomes. **a, d** Control 4T1 and RAW 264.7 cells. **b, e** 4T1 and RAW 264.7 cells treated with exosomes-PalmReNL. **c, f** 4T1 and RAW 264.7 cells treated with CD63-mScarlet-exosomes. Punctate fluorescence signals were merged with nuclei stained with Hoechst 33342. Scale bar, 15 μm. White arrows, PalmReNL- or CD63-mScarlet-exosomes. **g** PalmReNL-exosomes taken up by 4T1 cells in the presence of concanamycin-A or Chloroquine showed higher bioluminescence signals compared to control. Error bars, SD (n = 8), *, P < 0.03, ****, P < 0.0001. **h, i** Conventional pH titration curves of the normalized bioluminescence signals of exosomes- and MVs-PalmReNL. Error bars, SD (n = 5).

Proliferation of various cell types by treatment with EVs *in vitro*

To evaluate the physiological significance of cellular EV-uptake we analyzed the proliferation curves of various cell types (Raw 264.7, 4T1, lung fibroblasts, and AMSCs) when cultured for a period of 48 h with or without EVs (2.5×10^9) derived from 4T1 cells expressing PalmReNL. Interestingly, only the exosome-enriched fraction increased the proliferation rate of every one of the cell types tested. By contrast, MVs increased the proliferation rate only in RAW 264.7 cells (Fig. 4b). Both exosomes and MVs activated macrophages (clearly evident by the change in morphology of cell spreading and formation of dendrite-like structures) after 48 h of treatment (compare Fig. 4d, e with Fig. 4c).
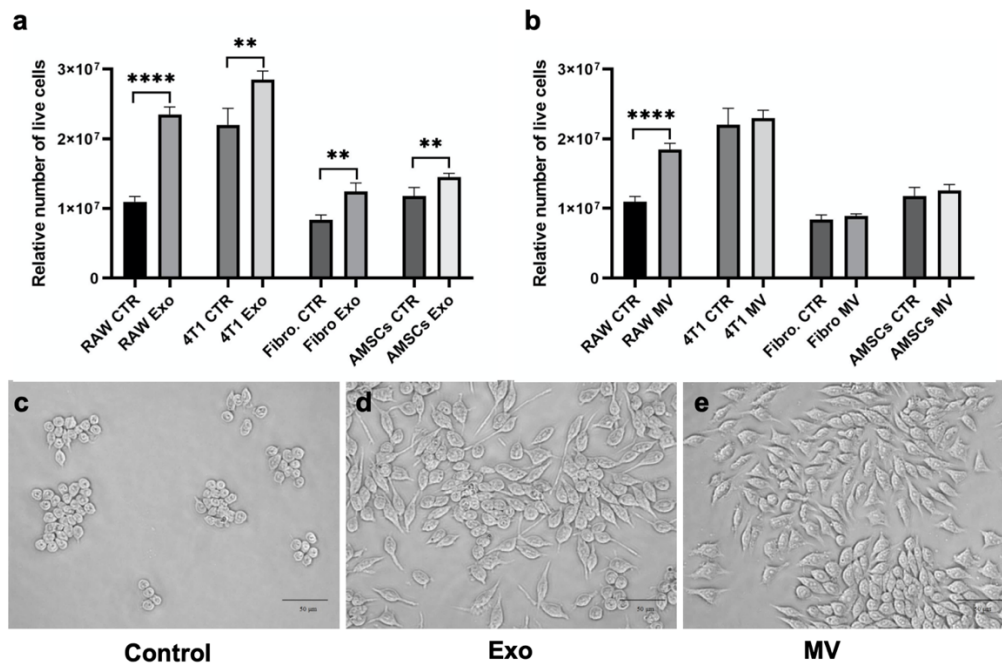
Fig. 4 Proliferation of various cell types by treatment with 4T1 cell-derived EVs *in vitro*. a, b Proliferation curves of various cell types (RAW 264.7 cells, 4T1 cells, lung fibroblasts and AMSCs) when cultured for a period of 48 h without or with EVs-PalmReNL (2.5×10^9). Error bars, SD (n = 4), **, P < 0.001; ****, P < 0.0001. **c, d, e** Both exosomes and MVs activated macrophages (clearly evident by the change in morphology) after 48 h of treatment. Scale bar, 50 μm.

232   **Exosomes and MVs derived from metastatic mammary carcinoma 4T1 cells**

233   **showed similar biodistribution and preferentially accumulated in the lung *in vivo*.**

234   To determine the biodistribution of 4T1 cell-derived exosomes and MVs, 1.0×10^9

235   exosomes or MVs carrying PalmReNL were administered intravenously (i.v.) in healthy

236   female BALB/c mice. Both reporter exosomes and MVs distributed throughout the body

237   within five min despite the difference of size and membrane composition between these

238   EV classes. The reporter exosomes displayed significantly higher bioluminescence

239   signals ($1.8 \times 10^6 \pm 8.8 \times 10^5$ p/s; n=18; p=0.0016; Fig. 5b, c, f) following i.v. injections,

240   compared to the reporter MVs i.v. injected ($1 \times 10^6 \pm 6.2 \times 10^5$ p/s; n=15; Fig. 5d, e, f).

241   The *ex vivo* signal, particularly in the lungs, was higher for the reporter exosomes ($3.0 \times$

242 $10^7 \pm 2.4 \times 10^7$ p/s; n=3; p=0.02; Fig. 5g), when compared to signal in lungs from control

243   mice ($3.9 \times 10^4 \pm 3.3 \times 10^4$ p/s; n=5; Fig. 5g). However, there was no significant difference

244   between the lung *ex vivo* signal for the reporter exosomes compared to that of the MVs

245   (Fig. 5g). Moreover, there were no significant differences between the bioluminescence

246   signals of the reporter exosomes and MVs injected i.p. (Fig. 5f).

247   The bioluminescence signals of the PalmReNL-exosomes and -MVs were also analyzed

248   in plasma samples collected at various time points (5 min, 2 h, 6 h, and 24 h) following

249   retro-orbital (i.v.) or i.p. injections (Fig. 5h and Supplementary Fig. 5). The maximum

250   bioluminescence signals were observed at 5 min in the i.v. injected reporter exosomes

251   and MVs. In contrast, it took 2 h to reach the maximum levels of the bioluminescence

252   signals in the i.p. injected reporter exosomes and MVs (Fig. 5h). The reporter MVs

253   showed total area under the curve (AUC) for i.v. $3.2 \times 10^8 \pm 5.7 \times 10^7$ p/s·h; n=15; and for

254   i.p. $3.2 \times 10^8 \pm 2.5 \times 10^7$ p/s·h; n=15; Fig. 5i). The reporter exosomes showed significantly

15

255 higher bioluminescence signals compared to the reporter MVs (total AUC for i.v. 9.6×10^8

256 $\pm 9.8 \times 10^7$ p/s·h; n=15; p=0.0006; for i.p. $7.2 \times 10^8 \pm 6.0 \times 10^7$ p/s·h; n=15; p=0.0005; Fig.

257 5i).

258 To determine if the bioluminescence signals of reporter MVs could be enhanced by

259 improved substrate availability *in vivo*[22], in the next set of experiments we tested a Fz

260 analog FFz. PalmReNL-MVs were i.p. injected as injection routes (i.v. vs i.p.) did not

261 affect the AUC of PalmReNL-MVs (Fig. 5i). Because of its improved solubility, a higher

262 dosage of FFz can be applicable, but here we injected the same dosage of 0.25 mg/kg

263 as Fz to compare their sinsitivities. PalmReNL-MVs administered i.p. exhibited 6-fold

264 more bioluminescence when FFz was i.v. injected as the substrate ($2.5 \times 10^6 \pm 3.4 \times 10^5$

265 p/s; n=5; p=0.0005) as compared to Fz ($4.2 \times 10^5 \pm 1.1 \times 10^5$ p/s; n=5; Supplementary

266 Fig. 6).

267
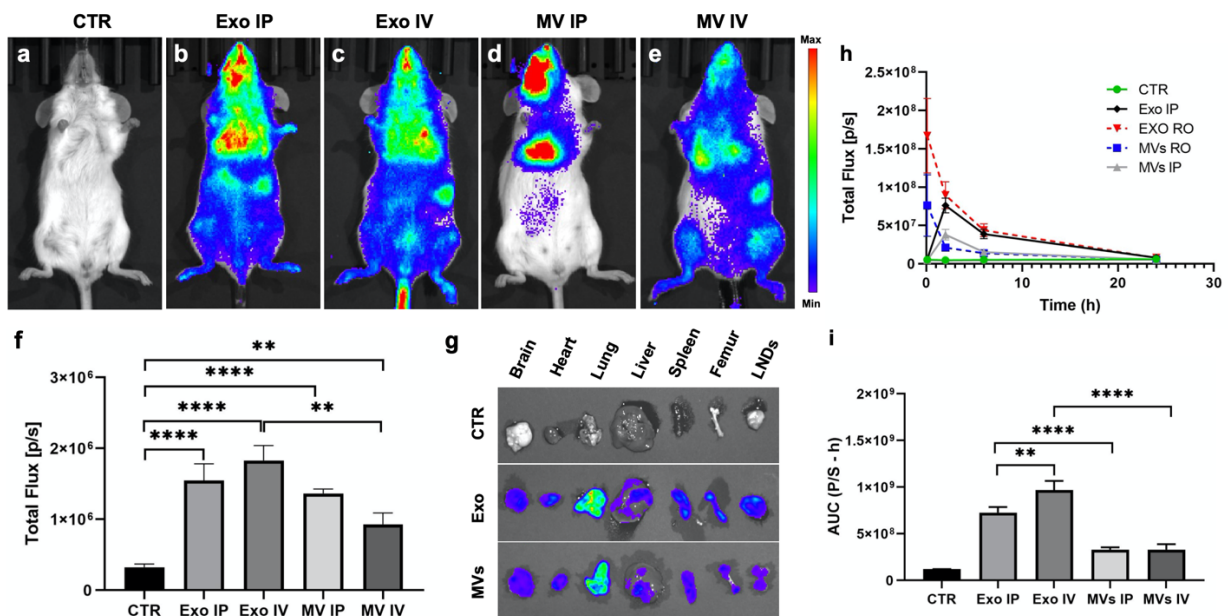
268

Fig. 5 Similar biodistribution and organotropism of exosomes and MVs derived from metastatic mammary carcinoma 4T1 cells. a-e 4T1 cell-derived exosomes and MVs, 1.0 x 10^9 PalmReNL-exosomes or -MVs were administered intravenously (i.v.) or intraperitonealy (i.p.) in healthy BALB/c mice. Furimazine was i.v. injected. **f** Analysis of bioluminescence signals in (a-e). There were no significant differences between the bioluminescence signals of PalmReNL-exosomes and -MVs injected i.p. **g** The *ex vivo* signal, particularly in the lungs, was higher for the reporter exosomes when compared to the signal in lungs from control mice. Error bars, SEM (CTR n =10; exosome i.p. n=3; exosome i.v. n=18; MV i.p. n=3; MV i.v. n=15), **, $P < 0.01$; ****, $P < 0.0001$. **h** The plasma samples were collected from the animals after EV isolation. The reporter exosomes displayed significantly higher bioluminescence signals compared to the reporter MVs in the plasma samples. The maximum bioluminescence signals were observed at 5 min in the i.v. injected reporter exosomes and MVs. In contrast, it took 2 h to reach the maximum levels of the bioluminescence signals in the i.p. injected reporter exosomes and MVs. Error bars, SD (n = 3). **i** AUC analysis of the bioluminescence signals in the plasma samples over 24 h post-EV injection. Error bars, SD (n = 15), **, $P < 0.01$; ****, $P < 0.0001$.

269

270 **Bioluminescence signals in tumor-bearing mice decreased as the tumors grow.**

271 Despite their distinct sizes and cellular origins, the reporter exosomes and MVs derived

272 from 4T1 cells behaved similarly *in vitro* and *in vivo* under the constraints of our

273 experimental approach. However, the PalmReNL-MVs produced and retained

274 significantly higher fluorescence signals compared to the PalmReNL-exosomes, in

275 extracellular spaces as well as the intracellular environment after being taken up by cells

276 likely due to their larger size. Tumor cell-derived MVs have been shown to play a key role

277 in cancer progression by transferring oncogenic receptors to neighboring cells in the

278 tumor microenvironment[30-32]. However, how tumor cell-derived MVs distribute throughout

279 the body and contribute to metastasis formation has not been determined. In an effort to

280 start deciphering the roles that MVs play under both physiological and pathological

281 conditions, in the next sets of *in vivo* experiments we followed the behavior of reporter

282 MVs in mice with or without mammary tumors.

283   Interestingly, the bioluminescence signals of PalmReNL-MVs were significantly lower in

284   tumor-bearing mice compared to the healthy mice (Supplementary Fig. 7). Two weeks

285   after tumor cell injection, the bioluminescence signal in PalmReNL-MVs injected i.p. was

286   2.2-fold lower [$8.7 \times 10^5 \pm 1.3 \times 10^5$ p/s; n=4; p=0.002 (Supplementary Fig. 7b,d)],

287   compared to control [$1.9 \times 10^6 \pm 1.6 \times 10^5$ p/s; n=4 (Supplementary Fig. 7a,d)].
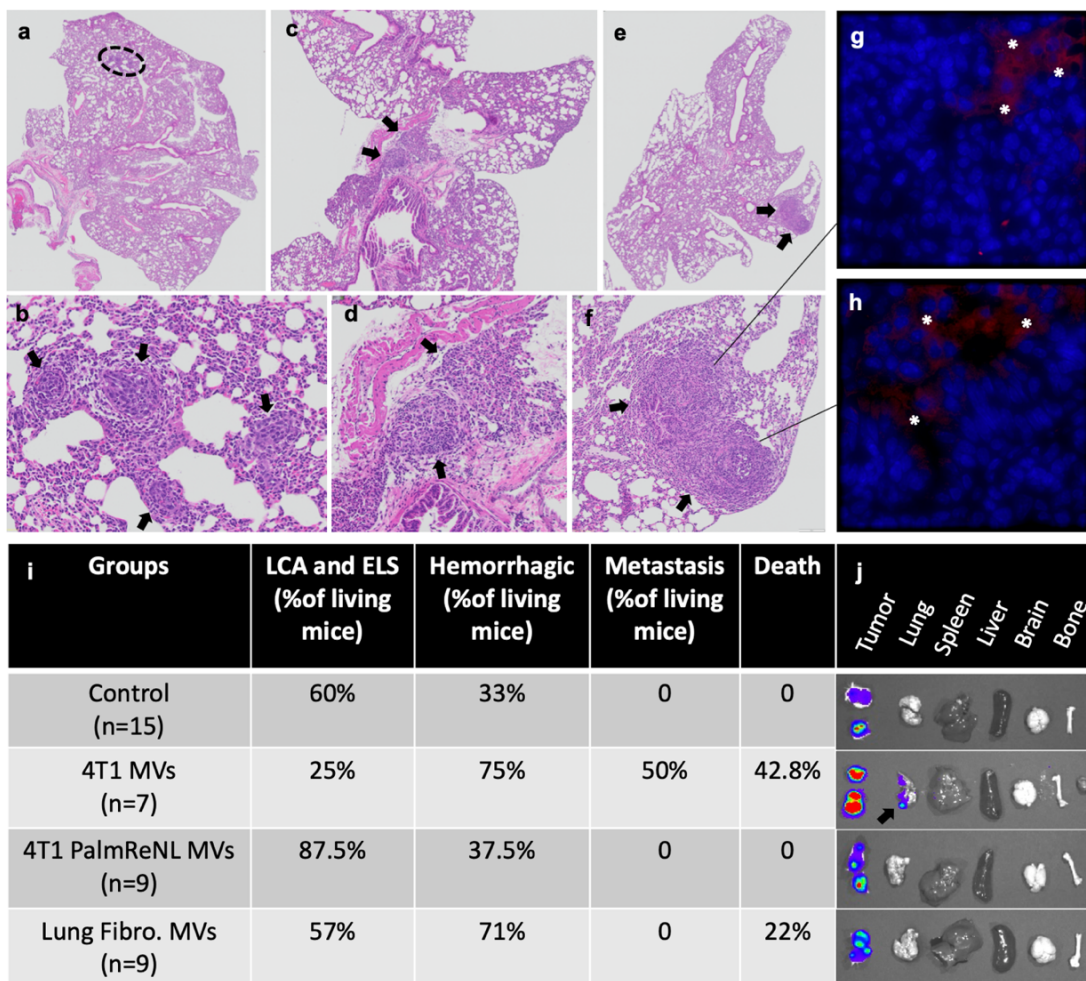
288

289   **Early induction of metastasis by multiple doses of tumor cell-derived MVs in**

290   **mammary tumor-bearing mice.**

291   The decrease of the bioluminescence signal of the reporter MVs in the presence of tumors

292   combined with the results of other *in vivo* and *in vitro* experiments suggest the

293   involvement of EV-mediated signaling pathways in the modulation of mammary tumor

294   progression, most probably at the level of the lungs. Therefore, in the next set of

295   experiments we investigated whether or not MVs play any role in the induction of

296   metastatic lesions.

297   One week after orthotopic injection of reporter 4T1-BGL cells constitutively expressing

298   fLuc and eGFP, 90% of immunocompetent BALB/c mice developed detectable tumors in

299   the mammary fat pad as revealed by bioluminescence imaging (BLI) (n=40). By two

300   weeks after injection of the reporter 4T1 cells, the tumors were still growing steadily.

301   Metastasis was evident in 50% of females that received multiple injections of MVs three

302   weeks after the tumor formation, but only when the MVs were purified from 4T1 cells (Fig.

303   6i). The metastatic foci were detected *ex vivo* using D-luciferin as the substrate (Fig. 6j;

304   arrow points to the fLuc bioluminescence signal detecting metastasis in the lung of a

305   mouse treated with 4T1 cell-derived MVs).

306   In addition, the metastatic foci were detected by histological analysis of lung sections

307   following H&E staining (Fig. 6a-f). EGFP-positive cells were observed only in areas near

308   the metastatic foci (Fig. 6g, h). Other histological findings included: hemorrhagic lungs

309   were more apparent in mice treated with MVs purified from fibroblasts (71%) and 4T1

310   cells (75%) compared to control tumor-bearing mice; the appearance of ectopic lymphoid

311   structures (ELS) or lymphoid cell aggregates (LCA)[33] were predominantly present in lungs

312   of mice treated with MVs isolated from 4T1 cells expressing PalmReNL (87.5%; Fig. 6i).

313   No other significant pulmonary lesions other than intravascular evidence of systemic

314   inflammation were observed.

| i Groups	LCA and ELS (%of living mice)	Hemorrhagic (%of living mice)	Metastasis (%of living mice)	Death	j
Control (n=15)	60%	33%	0	0	
4T1 MVs (n=7)	25%	75%	50%	42.8%	
4T1 PalmReNL MVs (n=9)	87.5%	37.5%	0	0	
Lung Fibro. MVs (n=9)	57%	71%	0	22%	

315

Fig. 6 Promotion of early metastasis by multiple doses of tumor cell-derived MVs in mammary tumor-bearing mice. a-f, H&E of mouse lung tissues depicting the metastatic foci from two mice treated with 4T1 cell-derived MVs. The images in (a, c, e) are enlarged in (b, d, f). Black arrows indicate metastatic foci. **g, h** GFP-positive cells (stars) from the primary mammary tumors were observed only in areas near the metastatic foci. **i** The table depicts other findings including: hemorrhagic lungs, ectopic lymphoid structures (ELS) or lymphoid cell aggregates (LCA), and death. **j** In *ex vivo* BLI data, an arrow points to metastatic foci of 4T1-BGL cells detected in the lung using D-luciferin.

316

317 The appearance of ELS and LCA structures within the lung suggested a strong

318 inflammatory response due to the administration of PalmReNL-MVs. We confirmed this

319 observation through performing immunohistochemistry of lung slides for the localization

320 of F4/80 positive cells to detect foci of inflammation and particularly cells of the

321 mononuclear phagocyte lineage[34]. As expected, cells positive for the F4/80 antigen were

322 primarily associated with the lungs of mice treated with MVs derived from 4T1 cells

323 expressing PalmReNL, localizing primarily to the bronchiolar epithelium and the

324 pulmonary interstitium (Fig. 7e). Intriguingly, lungs treated with 4T1 cell-derived MVs

325 demonstrated the most aggressive metastatic phenotype, while the F4/80 antigen did not

326 show a remarkable immune response.

327 This MV-mediated promotion of metastasis suggests that 4T1 cell-derived MVs may

328 modify the tissue microenvironment within the lung in a way that potentiates survival of

329 metastatic cells. Previous reports showed that EVs are released during stress and can

330 ultimately metabolically reprogram adjacent cells, promoting survival, invasion, and

331 metastasis[35,36]. We hypothesized that MVs may be potentiating the survival of cancer

332 cells within the lung through a similar mechanism. To assess the metabolic health within

333 the lung of MV-treated mice, we performed immunohistochemistry of the lung slides for

334   the localization of MAP1LC3B (LC3), a key autophagy player that is often upregulated to

335   promote cancer cell survival in the presence of metabolic stress[37]. Remarkably, the

336   expression of the LC3 was upregulated in the lung tissue of mice that developed early

337   metastasis following multiple injections of MVs purified from unmodified 4T1 cells (Fig.

338   7h).
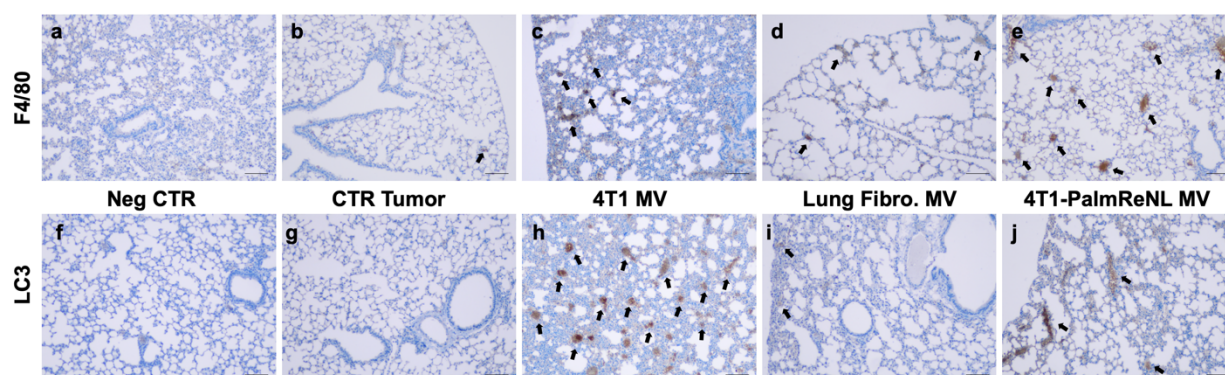
Fig. 7 Immunohistochemistry detection of inflammatory foci and the LC3B protein expression. a-e Tissue sections of lungs from the different experimental groups stained with anti-F4/80 antibodies. **f-j** Tissue sections of lungs stained with anti-LC3B antibodies. Scale bars, 100 μm. Black arrows indicate F4/80 or LC3 positive regions.

340

341   **Autophagy knockout cell lines exhibited increased EV release.**

342   Because metabolic stress promotes EV release, we investigated the possibility that it may

343   affect MV uptake and release. We tested this within U2OS cells, a well-characterized

344   autophagy model cell line[38], due to the stark LC3 upregulation seen in our lung metastasis

345   models. Unfortunately, traditional tools used to induce metabolic stress, such as

346   mitochondrial uncouplers or amino acid starvation, result in cell death within 24 hrs and

347   we were unable to accumulate sufficient MVs within the conditioned media at this

348   timepoint. Instead, we characterized the uptake and release of EVs within three different

21

349   cell lines lacking autophagy-related genes (Atg2A/B, Atg5, and Atg9A; Supplementary

350   Fig. 8), which are essential for the induction of LC3-dependent autophagy[39,40]. Cellular

351   uptake of PalmReNL-EVs was characterized by assessing tdTomato fluorescence and

352   measuring bioluminescence. Interestingly, authophagy KO cell lines had opposing effects

353   on the uptake and release of EVs. Atg2A/B, Atg5, and Atg9A KO had reduced uptake of

354   MVs derived from PalmReNL-4T1 cells at 24 h in U2OS cells as assessed by flow

355   cytometry (Fig. 8d and Supplementary Fig. 9), while bioluminescence signals exhibited

356   reliable results only at 2 h, possibly due to acid sensitivity of PalmReNL (Fig. 8g). The

357   uptake of exosomes was reduced mainly in Atg2A/B and Atg5 KO cell lines (Fig. 8b). On

358   the other hand, the release of MVs increased significantly in all the autophagy KO cell

359   lines (Fig. 8j). The release of exosomes increased at the 72 h time point in the Atg2 KO

360   cell line only (Fig. 8i).

361
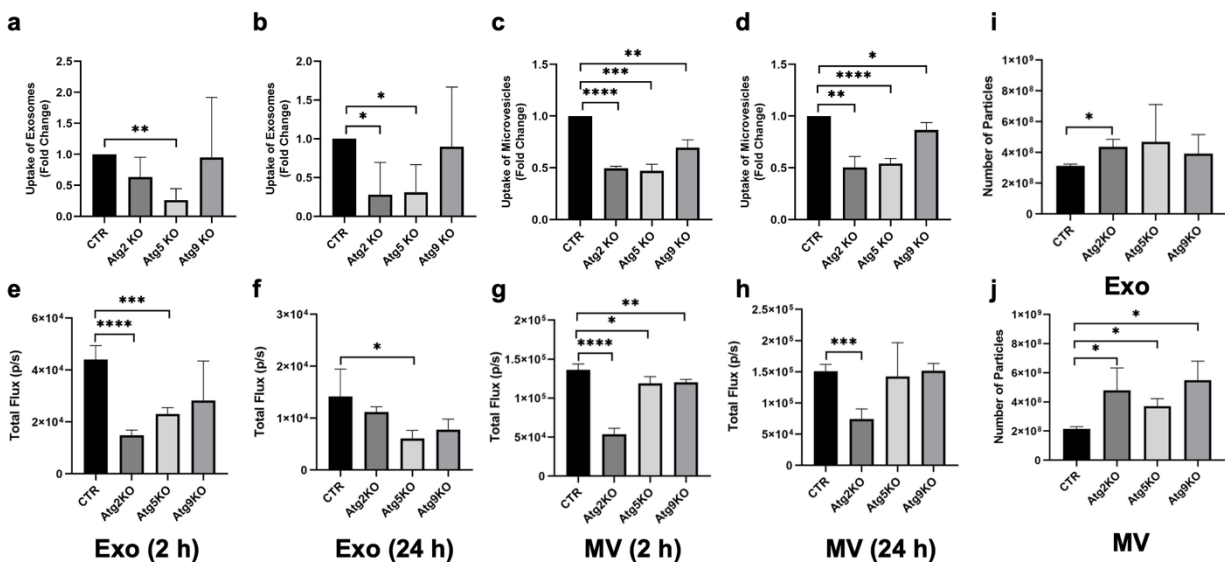
362

Fig. 8 Decreased EV uptake and incresed EV release by blocking autophagy *in vitro*. Uptake of PalmReNL-exosomes or -MVs in control and autophagy knockout (KO) cell lines, analyzed by flow cytometry and measuring bioluminescence. **a-d** Flow cytometric analysis of cellular uptake of PalmReNL-EVs (tdTomato$^+$) in U2OS Atg KO cells relative to control cells. The fold change of EV uptake was calculated using tdTomato fluorescence signals in KO cells compatred to the control (CTR). Error bars, SD (n = 3). **e-h** Uptake of PalmReNL-EVs determined by measuring bioluminescence signals. Error bars, SD (n = 4). **i** The release of exosomes assessed by NTA increased at the 72 h time point in the Atg2-KO cell line only. **j** The release of MVs increased significantly in all the autophagy KO cell lines. Error bars, SD (n = 3), *, P < 0.05; **, P < 0.01; ***, P < 0.001; ****, P < 0.0001.

363

Discussion

365 Our BRET-based EV reporter presents a new tool for understanding the roles played by

366 the distinct EV classes under physiological and pathological conditions. Using a novel

367 PalmReNL EV probe, we visualized two major classes of EVs, exosomes and MVs, *in*

368 *vitro* and *in vivo* under the constraints of current technologies for isolation and

369 characterization of EVs. Our BRET-based EV reporter presents as a new tool for

370 understanding the roles played by the distinct EV subtypes under physiological and

371 pathological conditions. In addition to allowing us to determine with high sensitivity the *in*

372 *vivo* biodistribution of exosomes and MVs, this EV reporter allowed us to decipher the

373 possible roles of mammary tumor-derived MVs in mediating metastasis to the lungs.

374 Although EV research remains restricted by current experimental limitations in separation

375 of EV classes, the size and molecular markers of the EV subtypes in this study support

376 the successful enrichment of exosomes and MVs in our experimental procedures[18,19].

377 The addition of PalmReNL into the EV membrane did not appear to impair the biological

378 functions of both exosomes and MVs, as demonstrated *in vitro* with the uptake

379 experiments using various cell lines, and *in vivo* biodistribution studies in mice. Of note,

380   PalmReNL-labeled MVs induced inflammatory responses in the lungs of the mammary

381   tumor-bearing immunocompetent mice. Technical limitations with the detection of cellular

382   uptake of PalmReNL-labeled exosomes gave the false impression of less uptake

383   compared to MVs. However, we demonstrated the lack of sufficient sensitivity for the

384   detection of fluorescence signals of PalmReNL in the recipient cells when tracking

385   exosomes carrying CD63-mScarlet (Fig. 3c, f). Moreover, our analysis of single EVs by

386   flow cytometry revealed that the fluorescence signals in PalmReNL-labeled exosomes

387   were lower than those of PalmReNL-labeled MVs, possibly attributable to their size

388   differences and/or symmetrical labeling of MV membranes. However, an equal number

389   of exosomes showed higher bioluminescence signals than MVs. This result may indicate

390   that PalmReNL can label more exosomes, while individual exosomes carry probe

391   molecules not detectable by flow cytometry due to the detection limit. Therefore, analysis

392   of bioluminescence signals may more appropriately reflect EV uptake in recipient cells.

393   We concluded that the Palm-based fluorescent EV probe is not ideal for tracking the fate

394   of small EVs (i.e., exosomes) in recipient cells. Rapid diffusion of PalmReNL in

395   endosomal network likely occurs after the cellular uptake of the reporter EVs, and the

396   level of fluorescence signals goes below background. We demonstrated that the EV

397   reporter may be processed through the endosomal-lysosomal pathway by using an acid-

398   insensitive reporter. PalmGamillus-exosomes retained the fluorescence signals in the

399   recipient cells compared to the PalmReNL-exosomes. Moreover, neutralizing the

400   endosomal pH increased the bioluminescence signal intensity of PalmReNL-exosomes.

401   Recently, the heterogeneity of EVs was well-documented[41]. Therefore, it was not

402   surprising that we found differences between the proliferation effects of exosomes and

403 MVs. The signals of EVs differed most likely because of their various surface receptors

404 and cargo. Additionally, recipient cells may have different activities of macropinocytosis

405 and multiple modes of receptor-mediated endocytosis[42,43]. Interestingly, unlike other cell

406 types tested, macrophage RAW 264.7 cells took up PalmReNL-MVs via clathrin- and

407 caveolin-dependent pathways (Fig. 2m, q). In addition to phagocytic and macropinocytic

408 EV uptake, this result corroborates findings that tumor cell-derived EVs are taken up

409 efficiently by macrophages *in vivo*[44,45].

410 In mice, the reporter-tagged exosomes and MVs showed similar *in vivo* biodistribution

411 with respect to their blood circulation and organotropism, primarily towards the lungs. The

412 analysis of the blood plasma also demonstrated that both types of EVs are quickly taken

413 up and by 6 h after injection, their blood levels had decreased by half. Interestingly, the

414 circulation time of the reporter MVs becomes shorter as tumors grow, possibly reflecting

415 the involvement of immune responses[44,46] as well as regulation orchestrated by the tumor

416 and the establishment of premetastatic niches[45,47,48]. A study has described how MVs

417 from metastatic melanoma cells enhance lung colonization of less aggressive, non-

418 metastatic melanoma cells[49]. However, further work on MVs has mainly highlighted the

419 ability of MVs to support primary tumor growth and survival[30,31,35]. The early appearance

420 of metastatic foci observed in the present studies following multiple MV injections

421 document potent far-reaching effects mediated by tumor cell-derived MVs and support

422 their future potential as theranostic agents[11,50]. Our *in vitro* assays demonstrated that EVs

423 can trigger biological responses in lung fibroblasts, AMSCs, macrophages, as well as in

424 epithelial cells. Any one of these cells, if not all, could be involved in the preparation of

425 the cell niche that favors metastasis to the lungs during repeated MV injections, a

426   hypothesis that awaits confirmation. Importantly, in the present studies, MVs derived from

427   normal tissues did not appear to contribute to the development of metastatic disease.

428   A better understanding of the EV-mediated systemic cross-talk between tumor cells and

429   distant cells should aid in developing novel therapeutic approaches. For example, in lung

430   and liver metastasis, exosomes exert their effect through immune cells and stromal

431   cells[45,51]; in the bone, they mainly modulate local stromal cells, osteoclasts, and

432   osteoblasts[52,53]. In liver metastasis of pancreatic cancer, macrophages play an essential

433   role in receiving and relaying signals from tumor cell-derived exosomes[45]. Based on these

434   studies, we hypothesized that MVs modulate metastatic behavior by orchestrating

435   changes in the local tumor microenvironment as well as the systemic activation and

436   recruitment of inflammatory cells at distant metastatic sites. However, results from our

437   experiments demonstrated that the inflammatory cells, likely interstitial macrophages,

438   appear to be more involved in prevention rather than in the promotion of early metastasis

439   (Fig. 7). It is likely that the MV-mediated potentiation of metastasis is multifactorial. This

440   is partially confirmed through the positiviely stained pockets of LC3 found within the lung

441   tissue, which demonstrate difference in autophagic signaling within the lung. We

442   hypothesize that tumor-derived MVs are modifying the tissue microenvironment within the

443   lung through metabolic reprogramming. This alteration can promote proliferation, survival,

444   and immune evasion of metastatic cancer cells in the regions they accumulate. However,

445   further studies are required to characterize whether the upregulation of LC3 is a direct or

446   indirect effect of MV administration. In addition, the influence of autophagy-related gene

447   knockout on the release and uptake of EVs will need further characterization as well.

448   In summary, our new BRET EV reporter system enabled us to track EVs *in vitro* and *in*

449   *vivo* with sufficient sensitivity. By combining non-invasive *in vivo* bioluminescence

450   imaging with molecular and cellular analyses, we deciphered the possible role of MVs

451   and LC3-associated mechanisms in early metastasis (summarized in Supplementary Fig.

452   10). Because of the complexity, EV-mediated signaling likely involves multiple pathways

453   depending on variations of cell types and physiological/pathological conditions.

454   Therefore, further extensive studies are needed to establish commonalities and functional

455   differences of the EV classes. The ability to non-invasively image cancer-associated

456   molecular markers will ultimately permit earlier detection and phenotyping of cancer,

457   making possible the development of targeted therapies specific for individual patients.

458

459   **Methods**

460   **Plasmid DNA constructs**

461   All plasmids were constructed using standard PCR cloning protocols. The constructs

462   were sequenced by GENEWIZ (South Plainfield, NJ) before using them for our

463   experiments. For stable reporter gene expression, we constructed a Sleeping

464   Beauty transposon[54], in which the reporter genes were under control of the CAG

465   promoter, by subcloning it into the multiple cloning site of the pKT2/CAGXSP vector[19]

466   through recombination cloning (In-Fusion HD Cloning Kit, Clontech). For the EV reporter,

467   a palmitoylation sequence (MLCCMRRTKQ) of GAP-43[15,55] was genetically fused to the

468   NH_2 terminus of NanoLuc[56] (PalmNLuc), Red-eNanoLantern (ReNL[16]; Addgene plasmid

469   #89536, gift from Takeharu Nagai), and Gamillus[26] for EV membrane anchoring by PCR

470   as reported previously. PalmNanoLuc and PalmReNL were amplified by PCR using

27

471   (forward)   5'   -

472   tggtggaattctgcagatagccgccaccATGCTGTGCTGTATGAGAAGAACCAAACAGGTCTTC

473   ACACTCGAAGATTTCGTTGGGGAC   and   (reverse)   5'   -

474   cgccactgtgctggatTTACGCCAGAATGCGTTCGCAC,   and   (forward)   5'   -

475   tggtggaattctgcagatagccgccaccATGCTGTGCTGTATGAGAAGAACCAAACAGGTGAGC

476   AAGGGCGAGGAGGTC   and   (reverse)   5'   -

477   cgccactgtgctggatTTACGCCAGAATGCGTTCGCAC,   respectively.   Human   CD63

478   (Addgene plasmid #62964, gift from Paul Luzio) and mScarlet[25] (Addgene plasmid

479   #85042,   gift   from   Dorus   Gadella)   were   amplified   using   (forward)   5'   -

480   tggaattctgcagatagccgccaccATGGCGGTGGAAGGAGGAATGAAATG

481   and   (reverse)   5'   -

482   ccaccgctacctccacctcctagatctccCATCACCTCGTAGCCACTTCTGATACTCTTC,   and

483   (forward)   5'   -tggaggtagcggtggaggtggaagccaggatccgATGGTGAGCAAGGGCGAGGC

484   and   (reverse)   5'   -gccactgtgctggatTTACTTGTACAGCTCGTCCATGCCG,   followed   by

485   combining these amplicons to generate CD63-mScarlet by overlap extension PCR. The

486   sequence of Gamillus was synthesized as gBlocks (IDT) and a palmitoylation sequence

487   was   fused   by   PCR   using   (forward)   5'   -

488   tggtggaattctgcagatagccgccaccATGCTGTGCTGTATGAGAAGAACCAAAC and (reverse)

489   5' -cgccactgtgctggatTTACTTGTACAGCTCGTCCATGCCG.

490

491   **Cell culture**

492   The labeling efficiency of the palmitoylated reporter was assessed in isolated fractions of

493   exosomes and MVs from PalmReNL- or PalmNanoLuc-expressing 4T1 cells. The murine

494   breast cancer 4T1 cells, murine macrophage Raw 264.7 cells, and primary mouse lung

495   fibroblasts were cultured in DMEM supplemented with GlutaMAX (Gibco), 10% (vol/vol)

496   FBS, and 1% penicillin/streptomycin. Mouse adipose-derived mesenchymal stromal cells

497   (AMSCs) were cultured in α-DMEM supplementd with 15% FBS and 1%

498   penicillin/streptomycin. Mouse primary lung fibroblasts and AMSCs were isolated as

499   previously described[57]. Monoclonal human osteosarcoma cell (U2OS 3XFlag-HaloTag-

500   Atg9A, see below) were cultured in RPMI media (Gibco/ThermoFisher, A4192301)

501   supplemented with 10% FBS and 1% penicillin/streptomycin. All cell cultures were

502   incubated at 37°C in a 5% CO_2 atmosphere. Some cultures were treated with either

503   methyl-β-cyclodextrin (MβCD; 10 mM), chlorpromazine (10 μg/mL)[58], concanamycin-A

504   (0.5 nM), or chloroquine (50 μM). All reagents were purchased from Sigma.

505

Generation of the Atg knockout (KO) cell lines

507   A endogenously edited monoclonal human osteosarcoma cell line (U2OS 3XFlag-

508   HaloTag-Atg9A) was used as the parental cell line (D.B. and J.S., manuscript in

509   preparation) and subsequent knockout (KO) cell lines were generated by first ligating

510   each genes corresponding sgRNA sequences (Atg2A: CGCTGCCCTTGTACAGATCG,

511   Atg2B: ATGGACTCCGAAAACGGCCA, Atg5: AACTTGTTTCACGCTATATC, Atg9A:

512   aggatatTCGAGAGAAGAAG, FlagTag: atggactacaaagaccatga) into the pX330-U6-

513   Chimeric_BB-CBh-hSpCas9 backbone vector[59] (Addgene plasmid # 42230; gift from

514   Feng Zhang). These plasmids were co-transfected with GFP (pMAXGFP, Lonza), and

515   single cells were sorted by FACS into 96-well plates, then screened and characterized by

516   Western blot. In the case of the Atg9A-KO cell line, an additional flagTag sgRNA was

517   added when the parental cell line was transfected.

518

Cell proliferation assays

520   Cell lines were seeded in 96-well plates at a density of 5,000 cells per well, and 24 h later

521   treated with 3.0 x 10^9 exosomes or MVs. The viability of the cultures was determined 24

522   h and 48 h after EV treatments by using the CellTiter-Fluor cell viability assay kit from

523   Promega (G6080) following manufacturers instructions. The filters in the fluorescence

524   plate reader were set for AFC (380-400 nm excitation; and 505 nm emission).

525

EV Isolation

527   EV-depleted FBS was prepared by 18-h ultracentrifugation at 100,000 g, $4°C^{60}$. 4T1,

528   PalmReNL-4T1, or PalmNanoLuc-4T1 cells were seeded at 1.5 x 10^6 cells per 100-mm

529   cell culture dish. After 24 h the medium was replaced with EV-depleted medium and the

530   cells were cultured for an additional 48-72 h. At the end of this culture period, MV- and

531   exosome-enriched   fractions   were   isolated   as   described   previously[18,19].   Briefly,

532   conditioned medium was centrifuged at 600 g for 5 min to remove cells and debris. The

533   supernatant was centrifuged again at 2,000 g for 20 min at room temperature (RT) to

534   remove apoptotic bodies. More dense MVs were separated from the less dense

535   exosomes by centrifugation at 20,000 g for 60 min at $4°C$, using a refrigerated

536   microcentrifuge 5424 R (Eppendorf). Supernatants were filtered through 0.2 µm PES

537   membrane filters (Nalgene, 725-2520) with pressure to remove large vesicles. Exosomes

538   were collected by a size-based EV isolation method with modifications[19,61] using 50-nm

539   membrane filters (EMD Millipore, VMWP02500 or Whatman, WHA110603) with holders

540   (EMD Millipore, SX0002500). Briefly, holders with 50-nm membrane filters were

541   connected to a vacuum manifold (Qiagen), and washed with 5-10 mL of PBS buffer by

542   applying vacuum. Next, the remaining exosome-enriched EV fraction in the supernatant

543   were trapped on the membranes. When approximately 200-500 µL of sample remained,

544   the concentrated exosome fraction was carefully collected. All EVs were aliquoted and

545   stored at -80°C.

546

547   **Nanoparticle tracking analysis (NTA) and Zeta potential (ZP) measurement**

548   EVs (exosomes and MVs) derived from 4T1 cells stably expressing PalmReNL,

549   PalmNanoLuc, or without transfection were analyzed using the ZetaView Multiple

550   Parameter Particle Tracking Analyzer (Particle Metrix) following the manufacturer's

551   instructions. EVs were diluted 100- to 1,000-fold with PBS or deionized water for the

552   measurement of particle size and concentration. The ZP of EVs was measured after

553   resuspending the EVs in deionized water to a concentration of 8.0×10^7 particles/mL as

554   previously reported[62].

555

556   **Isolation of EV fractions by density gradient centrifugation**

557   Conditioned medium from 4T1 PalmReNL cells was collected and centrifuged (600 g for

558   5 min, followed by another centrifugation at 2,000 g for 20 min). The supernatant was

559   then loaded on top of a discontinuous iodixanol gradient (OptiPrep; Sigma D1556) of 5%,

560 10%, 20%, 30%, 40% and 50% layers[63]. The gradient was then ultracentrifuged at

561 100,000 g for 18 h at 4 °C. Six fractions were carefully collected from top to bottom,

562 washed twice with PBS and pelleted by ultracentrifugation at 100,000 g for 1 h at 4°C.

563 Efficiency, purity and concentration of the fractions were assessed by NTA and measuring

564 bioluminescence signals.

565

566 **Flow cytometric analysis of surface phosphatidylserine (PS) in exosomes and MVs,**

567 **and cellular uptake of EVs**

568 For the analysis of EV surface PS, 100 µL of exosome- or MV-fractions derived from 4T1

569 cells expressing PalmReNL were stained with CellTrace Violet (CTV; Thermo Fisher,

570 C34571), followed by removing free dye with a spin desalting column (BioVision, 6564).

571 CTV-stained EVs were resuspended to a concentration of 3.5 x 10^9 particles/mL in Hanks

572 balanced salt solution (HBSS). 10x Annexin V binding buffer (0.1 M HEPES pH 7.4, 1.4

573 M NaCl, 25 mM $CaCl_2$.) was added to the mixture (final concentration 1x), and incubated

574 with Annexin V-APC (BioLegend; 8 ug/mL) to a final concentration of 0.7 µg/mL for 3 h at

575 RT. At the end of the incubation period, the EVs were fixed with 2% paraformaldehyde

576 (PFA, methanol-free, prepared with 1x Annexin V binding buffer; final volume 400 µL) for

577 20 min at RT. Immediately afterwards, the samples were run in the Cytek Aurora spectral

578 cytometer in the MSU Flow Cytometry Core Facility. Signal threshold was set using the

579 CTV signal to trigger off of detector V3 (violet), in order to discern EV signal from

580 background. Buffer only and buffer with staining reagents were run as assay controls to

581 reliably assess EV signals.

582 The uptake of PalmReNL-EVs by the Atg KO cell lines was also analyzed by flow

583 cytometry. Cells were plated in 24-well plates at a density of 50,000 cells/well, 24 h later

584 the cells were switched to EV-depleted medium, and 1×10^9 EVs/well were added. After

585 24 h, medium was removed and the cells were washed with PBS, trypsinized and

586 harvested. Immediately, the cells were fixed (4% PFA for 20 min at RT) and analyzed by

587 flow cytometry for the fluorescence signal of tdTomato compared to unstained-cells

588 (negative control) or 4T1 cells stably expressing PalmReNL (positive control).

589 Flow cytometry data were analyzed with FCS Express v7 (De Novo Software). Gates

590 were drawn based on fluorescence minus one (FMO) controls.

591

Fluorescence microscopy and Bioluminescence measurements

593 The uptake of PalmReNL EVs by murine macrophages (RAW 264.7), 4T1 cells, primary

594 mouse lung fibroblasts, mouse AMSCs, or U2OS-Atg-KO cells was analyzed by

595 fluorescence microscopy and measuring bioluminescence signals. The cells were plated

596 in 96- or 24-well plates at a concentration of respectively 20,000 or 50,000 cells/well. 24

597 h later the cells were switched to EV-depleted medium and the reporter 4T1 cell-derived

598 PalmReNL-exosomes or -MVs were added at a concentration of 3.5×10^9 (for RAW

599 264.7, 4T1, lung fibroblasts, or AMSCs) or $1-3 \times 10^9$ (for Atg-KO cell lines) EVs/well. At

600 least three wells were analyzed for each treatment group (control, exosomes, MVs). The

601 cultures were allowed to proceed for 24 h. At the end of the incubation period the uptake

602 of the reporter was analyzed by fluorescence microscopy or measuring bioluminescence

603 signals after adding furimazine (Fz; 25 µM) using a VICTOR Nivo Multimode Plate Reader

604 or IVIS Lumina (PerkinElmer).

33

605 Phase contrast and fluorescence images of PalmReNL-4T1 cells, reporter EVs, or cells

606 that were treated with the reporter EVs were taken using All-in-one Fluorescence

607 Microscope BZ-X700 (KEYENCE) or DeltaVision Microscope (GE Healthcare Life

608 Sciences). The cells were stained with 10 µg/mL Hoechst 33342 (H3570, Life

609 Technologies) before microscopy was performed. All images were further analyzed using

610 the ImageJ software (imagej.nih.gov).

611

Western blotting

613 Whole cell lysates and equal numbers of EVs (3.75×10^8 EVs) were derived from

614 unmodified 4T1 and PalmReNL-4T1 cells, and mixed with 4x sample buffer (Bio-Rad)

615 with β-mercaptoethanol (for detecting TSG101, ALIX, Flotillin-1, and anti-RFP) or without

616 β-mercaptoethanol (for detecting CD63). Proteins were separated on a 4%–20% Mini-

617 PROTEAN TGX gel (Bio-Rad) and transferred to a polyvinylidene difluoride membrane

618 (Millipore, IPFL00010). After blocking with 5% ECL Blocking Agent (GE Healthcare,

619 RPN2125) at RT for 1 h, membranes were probed with primary antibodies overnight at

620 4°C at dilutions recommended by the suppliers as follows: anti-Alix (Proteintech, 12422),

621 TSG101 (Proteintech, 14497-1-AP), flottilin-1 (BD, 610820), anti-RFP (Rockland

622 Immunochemicals, 600-401-379), CD63 (Thermo Fisher Scientific, 10628D, Ts63),

623 Atg2A (Cell Signaling, 15011), Atg2B (Cell Signaling, 25155), Atg5 (Cell Signaling,

624 12994), Atg9 (Cell Signaling, 13509), followed by incubation with horseradish peroxidase

625 HRP conjugated secondary antibodies at RT for 1 hour. The membranes were visualized

626 with ECL select Western Blotting Detection Reagent (GE Healthcare, RPN2235) on

627 ChemiDoc MP Imaging System (Bio-Rad).

34

628

Dot blot analysis

630   Membrane orientation of PalmReNL in EVs was characterized as reported previously[15].

631   Both exosomes and MVs carrying PalmReNL (3×10^7 EVs/μL) were 2-fold serially diluted.

632   Aliquots were incubated in the presence or absence of 1% Triton X-100 for 30 min at 37

633   °C. After pre-wetting a polyvinylidene difluoride membrane (Millipore, IPFL00010) in

634   methanol and equilibrating in transfer buffer, 2 μL of diluted EVs were dotted onto the

635   membrane and blocked in 5% non-fat dry milk (RPI, M17200-1000.0) for 1 h at room

636   temperature. The PalmReNL was detected using anti-RFP (Rockland Immunochemicals,

637   600-401-379) as described under Western blotting methods.

638

Proteinase K protection assay

640   Exosomes and MVs carrying PalmReNL were split into 3 identical aliquots (3×10^7

641   EVs/μL). Proteinase digestion was performed with 1 mg/mL proteinase K (Qiagen) in the

642   presence or absence of 1% Triton X-100 for 30 min at 37 °C as reported previously[64]. At

643   the end of a digestion period bioluminescence signals were measured after adding Fz (25

644   μM) using IVIS Lumina (PerkinElmer).

645

Transmission electron microscopy

647   The samples were prepared as previously reported[61], with slight modifications. Isolated

648   EVs (PalmReNL-exosomes: 6 x 10^7 EVs/μL, PalmReNL-MVs: 7×10^7 EVs/μL) were fixed

649 in 1% paraformaldehyde. A formvar-coated gold grid was kept in a saturated water

650 environment for 24 h, and placed on a 50 µL aliquot of EV solution, and allowed to

651 incubate for 20 min while covered. Next, samples were washed and blocked by placing

652 each one face down on top of a 100 µL droplet of the following solutions: PBS (2x, 3 min),

653 PBS / 50 mM Glycine (4x, 3 min), PBS / 5% BSA (1x, 10 min). A1:100 dilution of anti-

654 RFP antibody (Rockland Immunochemicals, 600-401-379) in 5% BSA / PBS was used

655 for labeling (1 h), followed by six washes in PBS / 0.5% BSA. Samples were incubated in

656 a 1:50 dilution of donkey anti-rabbit immunogold conjugate (Jackson ImmunoResearch,

657 711-205-152) in 5% BSA / PBS (20 min) and washed in PBS (6x) and water (6x). The

658 samples were negative stained with 1% uranyl acetate. Excess uranyl acetate was

659 removed by contacting the grid edge with filter paper and the grid was air-dried. Samples

660 were observed using a JEOL 1400 Flash Transmission Electron Microscope equipped

661 with an integrated Matataki Flash sCMOS bottom-mounted camera. The 1400 Flash

662 was operated at 100 kV.

663

664 **Bioluminescence pH titrations**

665 Bioluminescence signals in exosomes and MVs (3×10^7 EVs/µL) carrying PalmReNL

666 were measured at room temperature (25°C) using a VICTOR Nivo Microplate Reader

667 (PerkinElmer). EVs were incubated in the presence or absence of 1% Triton X-100 for 30

668 min at 37°C. The solutions consisted of 25 mM pH buffer, 125 mM KCl, 20 mM NaCl, 2

669 mM $CaCl_2$, and 2 mM $MgCl_2$ as reported[65]. The following buffers were used to adjust pH:

670 pH 4.0 – 5.0: Acetate Buffer; pH 5.5 – 6.5: MES Buffer; pH 7.0 – 8.0: HEPES Buffer.

671

In vivo tumor and metastasis studies

All procedures performed on animals were approved by the Institutional Animal Care and Use Committee of Michigan State University (East Lansing, MI). All mice were purchased from Charles River Laboratory. Eight week old female BALB/c mice with or without mammary tumors were used for the biodistribution studies of 4T1-PalmReNL-EVs (1.0 x 10^9 particles/100 uL). For the induction of tumors, 2.5 x 10^4 4T1 cells constitutively expressing BSD-eGFP and fLuc (BGL) were orthotopically injected into the mammary fat pads of female mice under anesthesia. For the studies analyzing the development of metastasis, following tumor induction, MVs (3.0 x 10^9 particles/100 uL) were injected into mice 3 times per week for 3 weeks (8 treatments in total). 4T1-BGL tumors were imaged (IVIS Spectrum system, see below) after i.p. injecting D-luciferin (3 mg/mouse in 100 µL PBS). Two weeks after tumor/metastasis induction the mice were imaged with the fluorofurimazine (FFz[22]) substrate (5 µg/mouse in 100 µL PBS), and the following day *in vivo* and *ex vivo* fLuc imaging were performed to analyze metastases. Immediately after, mice were sacrificed, dissected, and tissues were fixed (in neutral buffered formalin) and processed for histological analysis following paraffin embedding and H&E staining.

688

Lung immunohistochemistry

Immunohistochemistry for detection of the LC3 protein and the macrophage marker F4/80 was carried out using standard protocols. Briefly, unstained sections of lungs or tumors were deparaffinized and rehydrated, and then incubated in the peroxidase blocking

693   reagent (BioVision cat #K405-50). Antigen retrieval was perfomed by boiling the sections

694   in sodium citrate for 20 min. To decrease background staining, the slides were incubated

695   for 1 h in the mouse on mouse blocking reagent (Vector Labs MKB-2213-1), followed by

696   overnight incubation with the primary antibodies (LC3B Cell Signaling 3868S rabbit

697   polyclonal, 1:300; or F4/80 Cell Signaling 70076S rabbit monoclonal, 1:200). Next day,

698   the slides were washed and incubated with One-Step HRP polymer (BioVision cat #K405-

699   50) for 30 min at RT. The slides were then washed several times and then incubated with

700   the DAB chromogen for 10 min at RT, followed by several washing steps and quick

701   counterstain with Hematoxylin. Slides were then mounted and visualized under the

702   upright microscope (Nikon).

703

704   **Bioluminescence imaging (BLI)**

705   Bioluminescence analysis of the reporter exosomes and MVs was preceded by treatment

706   of different concentrations of 4T1-PalmReNL-EVs (MVs and Exosomes) with 25 µM Fz

707   or FFz (Promega). *In vitro* uptake or *in vivo* assays for the biodistribution of the reporter

708   exosomes and MVs were imaged with IVIS Lumina or IVIS Spectrum systems (Xenogen

709   product line of PerkinElmer). For *in vitro* assays, Fz was added to cultures of 4T1 cells,

710   RAW 264.7 cells, lung fibroblasts, AMSCs, or U2OS-Atg-KO cells that were treated with

711   the reporter exosomes or MVs prior to BLI. For *in vivo* imaging, mice were anesthetized

712   with isoflurane using a SAS3 Anesthesia System (Summit Anesthesia Support) and an

713   EVAC 4 waste gas evacuation system (Universal Vaporizer Support). Mice were injected

714   retroorbitally (RO) or intraperitoneally (IP) with MVs or exosomes (1.0×10^9 particles/100

715   µL) with either single or multiple injections (metastasis studies). Five min after intravenous

716　EV injection, or 2 h after intraperitoneal (IP) EV injection, the mice were injected with

717　either D-luciferin [150 mg/kg; IP], Fz (0.25 mg/kg; RO), or FFz (0.25 mg/kg; RO), and

718　emitted photons were captured with IVIS as described previously[66]. Immediately after *in*

719　*vivo* imaging, the mice were sacrificed and organs were excised. Organs were washed in

720　PBS, treated with Fz, and imaged with the IVIS system. Bioluminescence signals were

721　analyzed and quantified using the software program Living Image (PerkinElmer).

722

Statistical analyses

724　All statistical analyses were performed with GraphPad Prism software

725　(GraphPadSoftware). Screening results were analysed by one-way ANOVA followed by

726　Tukey's post-hoc test. Student *t* test was performed for all data set and *p* values were

727　noted. Differences were considered to be statistically significant when the *p* value was

728　less than 0.05.

729

Author contributions

731　A.A.Z., G.I.P., M.K. conceived and designed the experiments. M.K. supervised the work.

732　A.A.Z., G.I.P., D.B., B.D., A.M., V.T., L.K.T., M.P.B., A.W. executed the experimental

733　work. A.A.Z., G.I.P., M.K. carried out the data interpretation and statistical analysis. J.H.,

734　J.R.W., T.A.K., M.H.B., J.S. provided reagents and technical advice. All authors

735　contributed to the writing of the manuscript.

736

Conflict of interest

738　The authors declare no conflicts of interest.

739

Acknowledgements

748

References

1   van Niel, G., D'Angelo, G. & Raposo, G. Shedding light on the cell biology of extracellular vesicles. *Nat Rev Mol Cell Biol* **19**, 213-228, doi:10.1038/nrm.2017.125 (2018).

2   Kanada, M., Bachmann, M. H. & Contag, C. H. Signaling by Extracellular Vesicles Advances Cancer Hallmarks. *Trends Cancer* **2**, 84-94, doi:10.1016/j.trecan.2015.12.005 (2016).

3   Lai, C. P. *et al.* Dynamic biodistribution of extracellular vesicles in vivo using a multimodal imaging reporter. *ACS Nano* **8**, 483-494, doi:10.1021/nn404945r (2014).

4   Pucci, F. *et al.* SCS macrophages suppress melanoma by restricting tumor-derived vesicle-B cell interactions. *Science* **352**, 242-246, doi:10.1126/science.aaf1328 (2016).

5   Yong, T. *et al.* Tumor exosome-based nanoparticles are efficient drug carriers for chemotherapy. *Nat Commun* **10**, 3838, doi:10.1038/s41467-019-11718-4 (2019).

761 6   Liang, Q. *et al.* The softness of tumour-cell-derived microparticles regulates their drug-
762   delivery efficiency. *Nat Biomed Eng* **3**, 729-740, doi:10.1038/s41551-019-0405-4 (2019).

763 7   Lenzini, S., Bargi, R., Chung, G. & Shin, J. W. Matrix mechanics and water permeation
764   regulate extracellular vesicle transport. *Nat Nanotechnol* **15**, 217-223, doi:10.1038/s41565-
765   020-0636-2 (2020).

766 8   Maas, S. L. N., Breakefield, X. O. & Weaver, A. M. Extracellular Vesicles: Unique
767   Intercellular Delivery Vehicles. *Trends Cell Biol* **27**, 172-188,
768   doi:10.1016/j.tcb.2016.11.003 (2017).

769 9   Jeppesen, D. K. *et al.* Reassessment of Exosome Composition. *Cell* **177**, 428-445 e418,
770   doi:10.1016/j.cell.2019.02.029 (2019).

771 10   Xu, R. *et al.* Extracellular vesicles in cancer - implications for future improvements in
772   cancer care. *Nat Rev Clin Oncol* **15**, 617-638, doi:10.1038/s41571-018-0036-9 (2018).

773 11   Bose, R. J. C. *et al.* Tumor Cell-Derived Extracellular Vesicle-Coated Nanocarriers: An
774   Efficient Theranostic Platform for the Cancer-Specific Delivery of Anti-miR-21 and
775   Imaging Agents. *ACS Nano* **12**, 10817-10832, doi:10.1021/acsnano.8b02587 (2018).

776 12   Lazaro-Ibanez, E. *et al.* Selection of Fluorescent, Bioluminescent, and Radioactive Tracers
777   to Accurately Reflect Extracellular Vesicle Biodistribution in Vivo. *ACS Nano* **15**, 3212-
778   3227, doi:10.1021/acsnano.0c09873 (2021).

779 13   Wu, A. Y. *et al.* Multiresolution Imaging Using Bioluminescence Resonance Energy
780   Transfer Identifies Distinct Biodistribution Profiles of Extracellular Vesicles and
781   Exomeres with Redirected Tropism. *Adv Sci (Weinh)* **7**, 2001467,
782   doi:10.1002/advs.202001467 (2020).

783   14   Wills, C. A. *et al.* Chemotherapy-Induced Upregulation of Small Extracellular Vesicle-
784   Associated PTX3 Accelerates Breast Cancer Metastasis. *Cancer Res* **81**, 452-463,
785   doi:10.1158/0008-5472.CAN-20-1976 (2021).

786   15   Lai, C. P. *et al.* Visualization and tracking of tumour extracellular vesicle delivery and
787   RNA translation using multiplexed reporters. *Nat Commun* **6**, 7029,
788   doi:10.1038/ncomms8029 (2015).

789   16   Suzuki, K. *et al.* Five colour variants of bright luminescent protein for real-time
790   multicolour bioimaging. *Nat Commun* **7**, 13718, doi:10.1038/ncomms13718 (2016).

791   17   Sung, B. H. *et al.* A live cell reporter of exosome secretion and uptake reveals pathfinding
792   behavior of migrating cells. *Nat Commun* **11**, 2092, doi:10.1038/s41467-020-15747-2
793   (2020).

794   18   Kanada, M. *et al.* Differential fates of biomolecules delivered to target cells via
795   extracellular vesicles. *Proc Natl Acad Sci U S A* **112**, E1433-1442,
796   doi:10.1073/pnas.1418401112 (2015).

797   19   Kanada, M. *et al.* Microvesicle-mediated delivery of minicircle DNA results in effective
798   gene-directed enzyme prodrug cancer therapy. *Mol Cancer Ther*, doi:10.1158/1535-
799   7163.MCT-19-0299 (2019).

800   20   Raposo, G. & Stoorvogel, W. Extracellular vesicles: exosomes, microvesicles, and friends.
801   *J Cell Biol* **200**, 373-383, doi:10.1083/jcb.201211138 (2013).

802   21   Morales-Kastresana, A. *et al.* Labeling Extracellular Vesicles for Nanoscale Flow
803   Cytometry. *Sci Rep* **7**, 1878, doi:10.1038/s41598-017-01731-2 (2017).

804   22   Su, Y. *et al.* Novel NanoLuc substrates enable bright two-population bioluminescence
805   imaging in animals. *Nat Methods* **17**, 852-860, doi:10.1038/s41592-020-0889-6 (2020).

806   23   Rothberg, K. G. *et al.* Caveolin, a protein component of caveolae membrane coats. *Cell* **68**,

807   673-682, doi:10.1016/0092-8674(92)90143-z (1992).

808   24   Qian, Z. M., Li, H., Sun, H. & Ho, K. Targeted drug delivery via the transferrin receptor-

809   mediated endocytosis pathway. *Pharmacol Rev* **54**, 561-587, doi:10.1124/pr.54.4.561

810   (2002).

811   25   Bindels, D. S. *et al.* mScarlet: a bright monomeric red fluorescent protein for cellular

812   imaging. *Nat Methods* **14**, 53-56, doi:10.1038/nmeth.4074 (2017).

813   26   Shinoda, H. *et al.* Acid-Tolerant Monomeric GFP from Olindias formosa. *Cell Chem Biol*

814   **25**, 330-338 e337, doi:10.1016/j.chembiol.2017.12.005 (2018).

815   27   Drose, S. & Altendorf, K. Bafilomycins and concanamycins as inhibitors of V-ATPases

816   and P-ATPases. *J Exp Biol* **200**, 1-8 (1997).

817   28   Al-Bari, M. A. A. Targeting endosomal acidification by chloroquine analogs as a

818   promising strategy for the treatment of emerging viral diseases. *Pharmacol Res Perspect*

819   **5**, e00293, doi:10.1002/prp2.293 (2017).

820   29   Robers, M. B. *et al.* A luminescent assay for real-time measurements of receptor

821   endocytosis in living cells. *Anal Biochem* **489**, 1-8, doi:10.1016/j.ab.2015.08.005 (2015).

822   30   Al-Nedawi, K. *et al.* Intercellular transfer of the oncogenic receptor EGFRvIII by

823   microvesicles derived from tumour cells. *Nat Cell Biol* **10**, 619-624, doi:10.1038/ncb1725

824   (2008).

825   31   Al-Nedawi, K., Meehan, B., Kerbel, R. S., Allison, A. C. & Rak, J. Endothelial expression

826   of autocrine VEGF upon the uptake of tumor-derived microvesicles containing oncogenic

827   EGFR. *Proc Natl Acad Sci U S A* **106**, 3794-3799, doi:10.1073/pnas.0804543106 (2009).

828   32   Feng, Q. *et al.* A class of extracellular vesicles from breast cancer cells activates VEGF

829   receptors and tumour angiogenesis. *Nat Commun* **8**, 14450, doi:10.1038/ncomms14450

830   (2017).

831   33   Colbeck, E. J., Ager, A., Gallimore, A. & Jones, G. W. Tertiary Lymphoid Structures in

832   Cancer: Drivers of Antitumor Immunity, Immunosuppression, or Bystander Sentinels in

833   Disease? *Front Immunol* **8**, 1830, doi:10.3389/fimmu.2017.01830 (2017).

834   34   Austyn, J. M. & Gordon, S. F4/80, a monoclonal antibody directed specifically against the

835   mouse macrophage. *Eur J Immunol* **11**, 805-815, doi:10.1002/eji.1830111013 (1981).

836   35   Antonyak, M. A. *et al.* Cancer cell-derived microvesicles induce transformation by

837   transferring tissue transglutaminase and fibronectin to recipient cells. *Proc Natl Acad Sci*

838   *U S A* **108**, 4852-4857, doi:10.1073/pnas.1017667108 (2011).

839   36   Wang, T. *et al.* Hypoxia-inducible factors and RAB22A mediate formation of

840   microvesicles that stimulate breast cancer invasion and metastasis. *Proc Natl Acad Sci U*

841   *S A* **111**, E3234-3242, doi:10.1073/pnas.1410041111 (2014).

842   37   Mizushima, N., Yoshimori, T. & Levine, B. Methods in mammalian autophagy research.

843   *Cell* **140**, 313-326, doi:10.1016/j.cell.2010.01.028 (2010).

844   38   Mauthe, M. *et al.* Chloroquine inhibits autophagic flux by decreasing autophagosome-

845   lysosome fusion. *Autophagy* **14**, 1435-1455, doi:10.1080/15548627.2018.1474314 (2018).

846   39   Mizushima, N. & Komatsu, M. Autophagy: renovation of cells and tissues. *Cell* **147**, 728-

847   741, doi:10.1016/j.cell.2011.10.026 (2011).

848   40   Levine, B. & Kroemer, G. Biological Functions of Autophagy Genes: A Disease

849   Perspective. *Cell* **176**, 11-42, doi:10.1016/j.cell.2018.09.048 (2019).

850   41   Willms, E., Cabanas, C., Mager, I., Wood, M. J. A. & Vader, P. Extracellular Vesicle

851   Heterogeneity: Subpopulations, Isolation Techniques, and Diverse Functions in Cancer

852   Progression. *Front Immunol* **9**, 738, doi:10.3389/fimmu.2018.00738 (2018).

853   42   Mulcahy, L. A., Pink, R. C. & Carter, D. R. Routes and mechanisms of extracellular vesicle

854   uptake. *J Extracell Vesicles* **3**, doi:10.3402/jev.v3.24641 (2014).

855   43   van Dongen, H. M., Masoumi, N., Witwer, K. W. & Pegtel, D. M. Extracellular Vesicles

856   Exploit Viral Entry Routes for Cargo Delivery. *Microbiol Mol Biol Rev* **80**, 369-386,

857   doi:10.1128/MMBR.00063-15 (2016).

858   44   Imai, T. *et al.* Macrophage-dependent clearance of systemically administered B16BL6-

859   derived exosomes from the blood circulation in mice. *J Extracell Vesicles* **4**, 26238,

860   doi:10.3402/jev.v4.26238 (2015).

861   45   Costa-Silva, B. *et al.* Pancreatic cancer exosomes initiate pre-metastatic niche formation

862   in the liver. *Nat Cell Biol* **17**, 816-826, doi:10.1038/ncb3169 (2015).

863   46   Caruso, S. & Poon, I. K. H. Apoptotic Cell-Derived Extracellular Vesicles: More Than Just

864   Debris. *Front Immunol* **9**, 1486, doi:10.3389/fimmu.2018.01486 (2018).

865   47   Peinado, H. *et al.* Melanoma exosomes educate bone marrow progenitor cells toward a pro-

866   metastatic phenotype through MET. *Nat Med* **18**, 883-891, doi:10.1038/nm.2753 (2012).

867   48   Hoshino, A. *et al.* Tumour exosome integrins determine organotropic metastasis. *Nature*

868   **527**, 329-335, doi:10.1038/nature15756 (2015).

869   49   Poste, G. & Nicolson, G. L. Arrest and metastasis of blood-borne tumor cells are modified

870   by fusion of plasma membrane vesicles from highly metastatic cells. *Proc Natl Acad Sci*

871   *U S A* **77**, 399-403, doi:10.1073/pnas.77.1.399 (1980).

872   50   Guo, M. *et al.* Autologous tumor cell-derived microparticle-based targeted chemotherapy
873   in lung cancer patients with malignant pleural effusion. *Sci Transl Med* **11**,
874   doi:10.1126/scitranslmed.aat5690 (2019).

875   51   Plebanek, M. P. *et al.* Pre-metastatic cancer exosomes induce immune surveillance by
876   patrolling monocytes at the metastatic niche. *Nat Commun* **8**, 1319, doi:10.1038/s41467-
877   017-01433-3 (2017).

878   52   Probert, C. *et al.* Communication of prostate cancer cells with bone cells via extracellular
879   vesicle RNA; a potential mechanism of metastasis. *Oncogene* **38**, 1751-1763,
880   doi:10.1038/s41388-018-0540-5 (2019).

881   53   Furesi, G., Rauner, M. & Hofbauer, L. C. Emerging Players in Prostate Cancer-Bone Niche
882   Communication. *Trends Cancer* **7**, 112-121, doi:10.1016/j.trecan.2020.09.006 (2021).

883   54   Mates, L. *et al.* Molecular evolution of a novel hyperactive Sleeping Beauty transposase
884   enables robust stable gene transfer in vertebrates. *Nat Genet* **41**, 753-761,
885   doi:10.1038/ng.343 (2009).

886   55   McCabe, J. B. & Berthiaume, L. G. Functional roles for fatty acylated amino-terminal
887   domains in subcellular localization. *Mol Biol Cell* **10**, 3771-3786,
888   doi:10.1091/mbc.10.11.3771 (1999).

889   56   Hall, M. P. *et al.* Engineered luciferase reporter from a deep sea shrimp utilizing a novel
890   imidazopyrazinone substrate. *ACS Chem Biol* **7**, 1848-1857, doi:10.1021/cb3002478
891   (2012).

892   57   Huang, S. *et al.* An improved protocol for isolation and culture of mesenchymal stem cells
893   from mouse bone marrow. *J Orthop Translat* **3**, 26-33, doi:10.1016/j.jot.2014.07.005
894   (2015).

895   58   Rejman, J., Oberle, V., Zuhorn, I. S. & Hoekstra, D. Size-dependent internalization of

896   particles via the pathways of clathrin- and caveolae-mediated endocytosis. *Biochem J* **377**,

897   159-169, doi:10.1042/BJ20031253 (2004).

898   59   Cong, L. *et al.* Multiplex genome engineering using CRISPR/Cas systems. *Science* **339**,

899   819-823, doi:10.1126/science.1231143 (2013).

900   60   Shelke, G. V., Lasser, C., Gho, Y. S. & Lotvall, J. Importance of exosome depletion

901   protocols to eliminate functional and RNA-containing extracellular vesicles from fetal

902   bovine serum. *J Extracell Vesicles* **3**, doi:10.3402/jev.v3.24783 (2014).

903   61   Liu, F. *et al.* The Exosome Total Isolation Chip. *ACS Nano* **11**, 10712-10723,

904   doi:10.1021/acsnano.7b04878 (2017).

905   62   Midekessa, G. *et al.* Zeta Potential of Extracellular Vesicles: Toward Understanding the

906   Attributes that Determine Colloidal Stability. *ACS Omega* **5**, 16701-16710,

907   doi:10.1021/acsomega.0c01582 (2020).

908   63   Kowal, J. *et al.* Proteomic comparison defines novel markers to characterize heterogeneous

909   populations of extracellular vesicle subtypes. *Proc Natl Acad Sci U S A* **113**, E968-977,

910   doi:10.1073/pnas.1521230113 (2016).

911   64   Banfer, S. *et al.* Molecular mechanism to recruit galectin-3 into multivesicular bodies for

912   polarized exosomal secretion. *Proc Natl Acad Sci U S A* **115**, E4396-E4405,

913   doi:10.1073/pnas.1718921115 (2018).

914   65   Katayama, H. *et al.* Visualizing and Modulating Mitophagy for Therapeutic Studies of

915   Neurodegeneration. *Cell* **181**, 1176-1187 e1116, doi:10.1016/j.cell.2020.04.025 (2020).

916   66   Stacer, A. C. *et al.* NanoLuc reporter for dual luciferase imaging in living animals. *Mol

917   Imaging* **12**, 1-13 (2013).

47

918   **Supporting Information**

919

920   *In vitro* and *in vivo* analysis of microvesicle-mediated metastasis using a
921   bright, red-shifted bioluminescent reporter protein of extracellular vesicles

922

923   **Authors**

924   Ahmed A. Zarea[*1], Gloria I. Perez[*1,2], David Broadbent[1,2], Benedikt Dolgikh[1,4], Matthew
925   P. Bernard[1,3], Alicia Withrow[8], Amelia McGill[1], Victoria Toomajian[1,5], Lukose K.
926   Thampy[1,2], Jack Harkema[3], Joel R. Walker[9], Thormas A. Kirkland[9], Michael H.
927   Bachmann[1,6], Jens Schmidt[1,7], and Masamitsu Kanada[**1,3]

928

929

930   **Affiliations**

931   [1]Institute for Quantitative Health Science and Engineering (IQ), [2]College of Osteopathic
932   Medicine, [3]Department of Pharmacology & Toxicology, [4]College of Natural Science,
933   [5]Department of Biomedical Engineering, [6]Department of Microbiology & Molecular
934   Genetics, [7]Department of Obstetrics and Gynecology, College of Human Medicine,
935   [8]Center for Advanced Microscopy, Michigan State University, East Lansing, Michigan.
936   [9]Promega Biosciences LLC, 227 Granada Dr, San Luis Obispo, CA.

937

938   *These authors contributed equally to this work.

939

940   **Correspondence and requiests for materials should be addressed to M.K. (email:
941   kanadama@msu.edu).

942

943

944
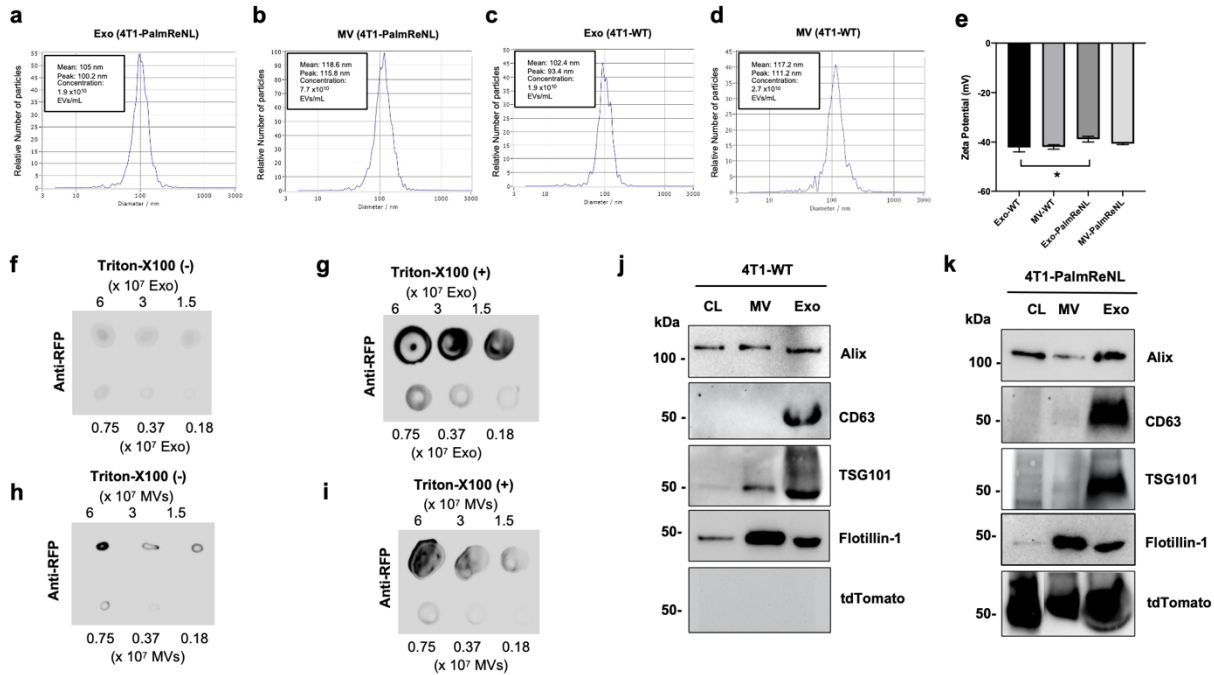
Zarea, Perez, et al.

Supplementary Figure 1. Characterization of 4T1 cell-derived PalmReNL-EVs. a-d 4T1 cell-derived PalmReNL-exosomes and -MVs were analyzed by nanoparticle tracking analysis (NTA). Exosomes and MVs derived from unmodified 4T1 cells were analyzed as control. **e** Determination of the Zeta potential revealed that the PalmReNL slightly shifted the surface charge of exosomes, but not MVs. Error bars, SD (n = 3), *, P < 0.05.
 f, g, h, i Dot blot assays for PalmReNL-exosomes and -MVs plus or minus Triton-X100. **j** Western blot analysis of exosome marker proteins of unmodified 4T1 cells, MVs, and exosomes. **k** Western blot analysis of exosome marker proteins of PalmReNL-4T1 cells, -MVs, and -exosomes.

49

970
971

a
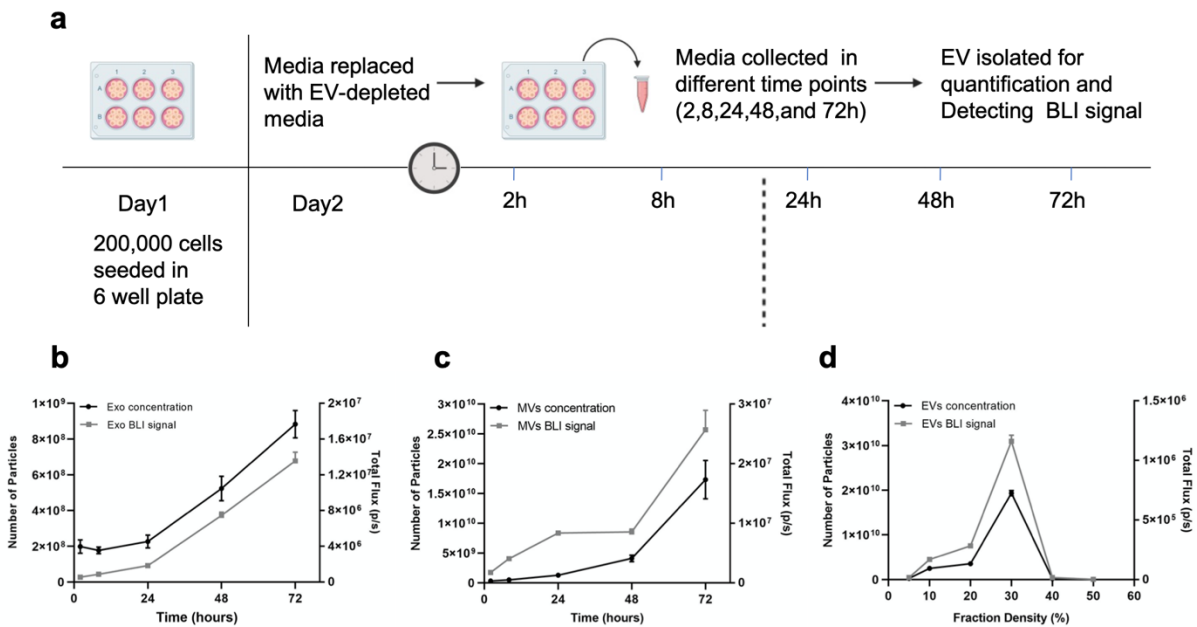
972
973
974
975
976
977

Supplementary Figure 2. Characterization of EV release from 4T1 cells *in vitro*. a Schematic representation of the sampling protocol. **b, c** The bioluminescent signals correlated with the number of particles present. **d** The bioluminescent signals were also correlateed with the number of EVs purified from different EV fractions after density gradient. Error bars, SD (NTA, n=3; BLI, n=9).

983
984
985
986
987
988
989
990
991
992
993
994

995
996
997
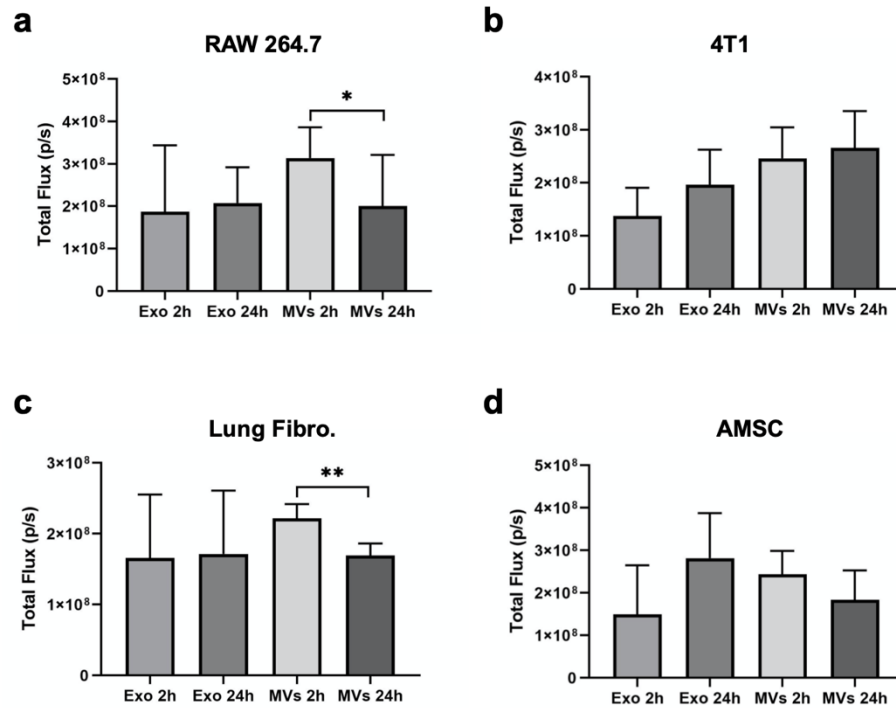
998
999
1000
1001
1002
1003
1004 **Supplementary Figure 3. Short-term and long-term cellular uptake of 4T1 cell-**
1005 **derived PalmReNL-exosomes and -MVs assessed by measuring bioluminescent**
1006 **signals. a** Macrophage RAW 264.7 cells. **b** 4T1 cells. **c** Mouse lung fibroblasts. **d** Mouse
1007 adipose-derived mesenchymal stromal cells (AMSCs). Error bars, SD (n = 8), *, P < 0.05;
1008 **, P < 0.01.

1009
1010
1011
1012
1013
1014
1015
1016
1017
1018
1019
1020
1021

1022
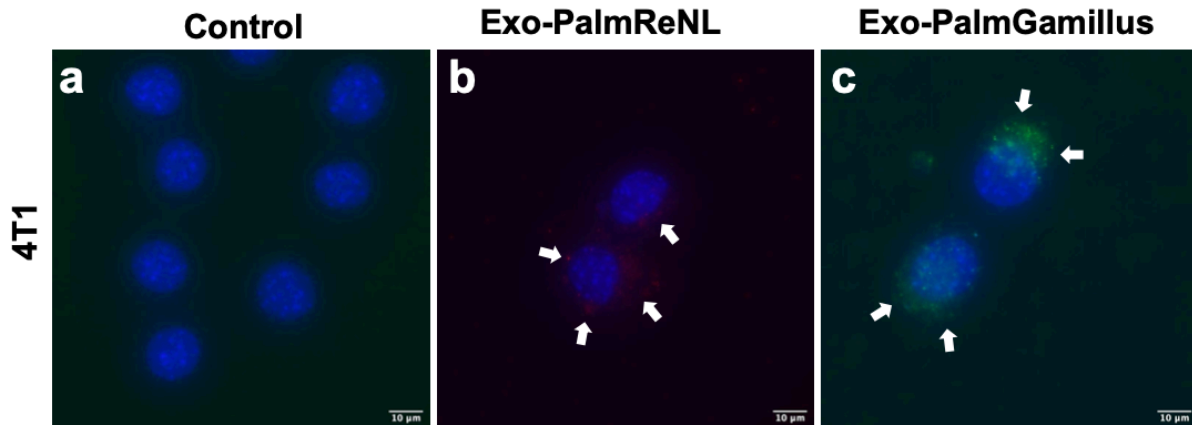
1023
1024
1025
1026
1027
1028
1029
1030
Supplementary Figure 4. Retained fluorescence signals of PalmGamillus-exosomes in the recipient cells compared to the PalmReNL-exosome signal which was barely detected. Fluorescence microscopy images of 4T1 cells treated for 24 h with PalmReNL- or PalmGamillus-exosomes. White arrows, PalmReNL- or -PalmGamillus-exosomes.

1036
1037
1038
1039
1040
1041
1042
1043
1044
1045
1046
1047
1048
1049
1050
1051
1052
1053
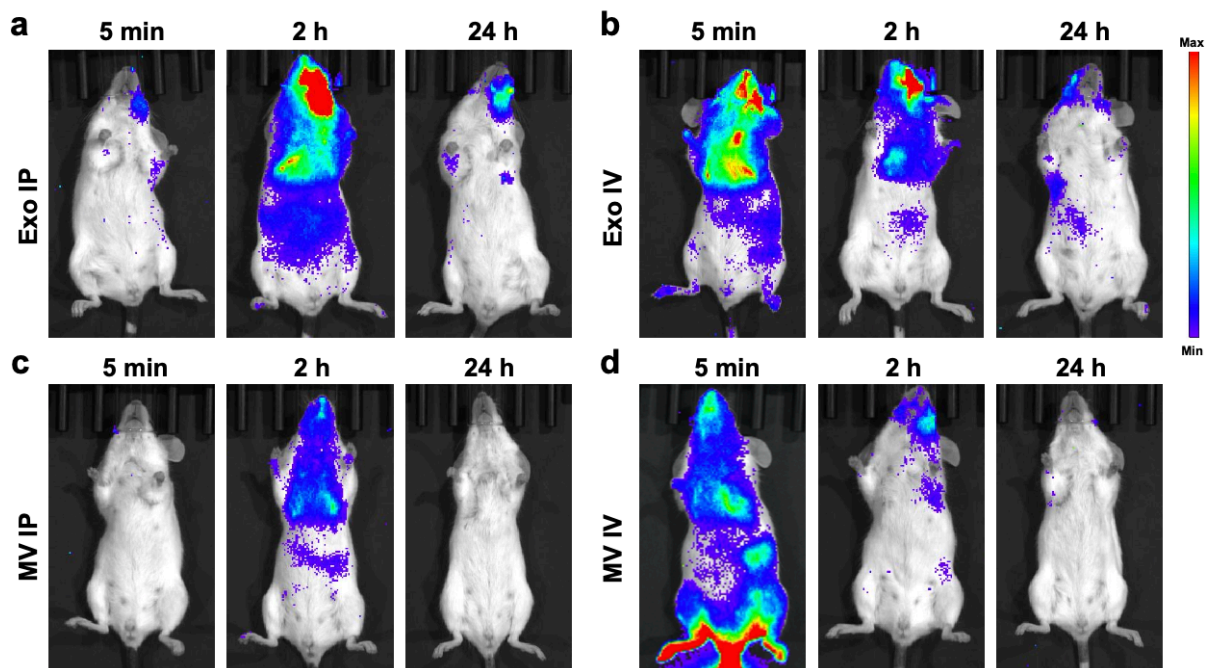
Supplementary Figure 5. Dynamic biodistributions of PalmReNL-exosomes and -MVs following retro-orbital (i.v.) or intraperitoneal (i.p.) injections. a-d Representative biodistributions of the reporter PalmReNL-EVs (n = 3). *In vivo* BLI at 5 min, 2 h, and 24 h after injecting reporter PalmReNL-exosomes and -MVs. Furimazine (Fz) was administered retro-orbitally.
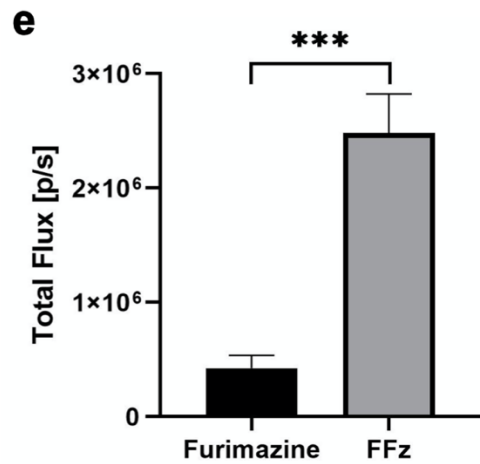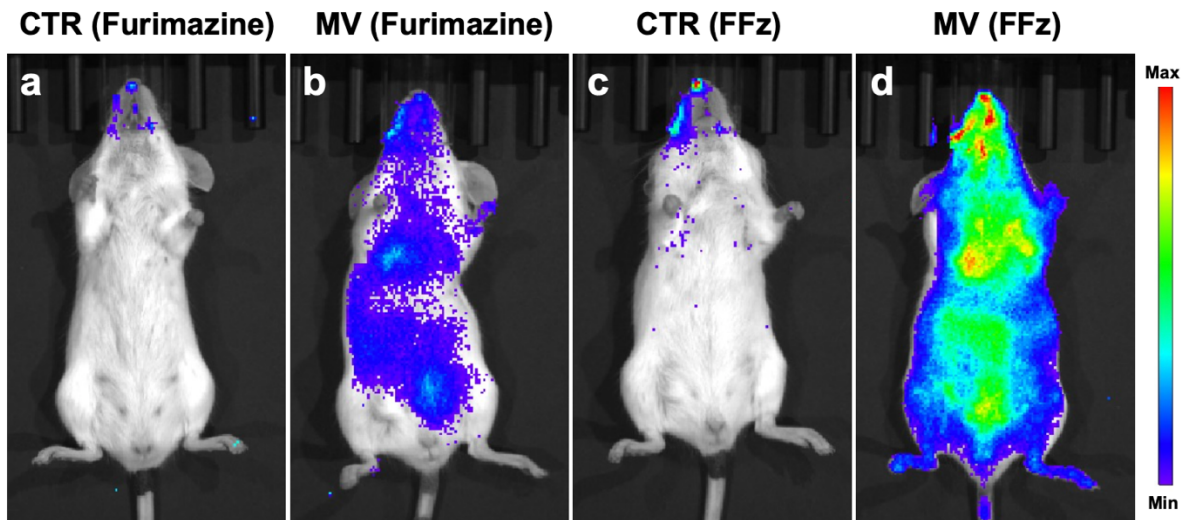
CTR (Furimazine) **MV (Furimazine)** **CTR (FFz)** **MV (FFz)**

Supplementary Figure 6. Enhanced bioluminescent signals of PalmReNL-MVs when Fluorofurimazine (FFz) was used as the substrate *in vivo*. a, c Control mice. **b, e** The bioluminescent signal of i.p. injected PalmReNL-MVs using furimazine as the substrate after. **d, e** The sensitivity of the reporter PalmReNL-MVs administered intraperitoneally was markedly increased when FFz was used as the substrate; Error bars, SEM (n = 5), ***, P < 0.001.

54
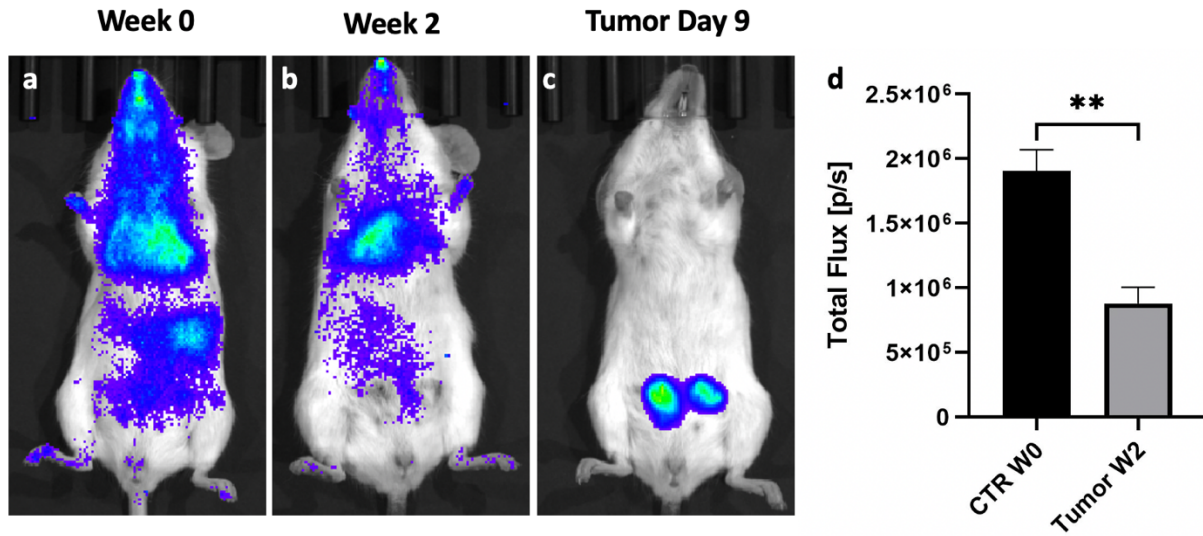
Supplementary Figure 7. Lower bioluminescent signals of the reporter MVs-PalmReNL detected in tumor-bearing mice compared to the healthy mice. Bioluminescent signals of the PalmReNL-MVs in mice with and without tumors. **a** Control mice. **b** Mammary tumor-bearing mice two week after tumor implantation. **c** Mammary tumor growth was assessed by fLuc BLI. **f** Quantitative analysis of the bioluminescent signals of PalmReNL-MVs *in vivo* for each one of the experimental groups. Error bars, SEM (n = 4), **, P = 0.002.

1125
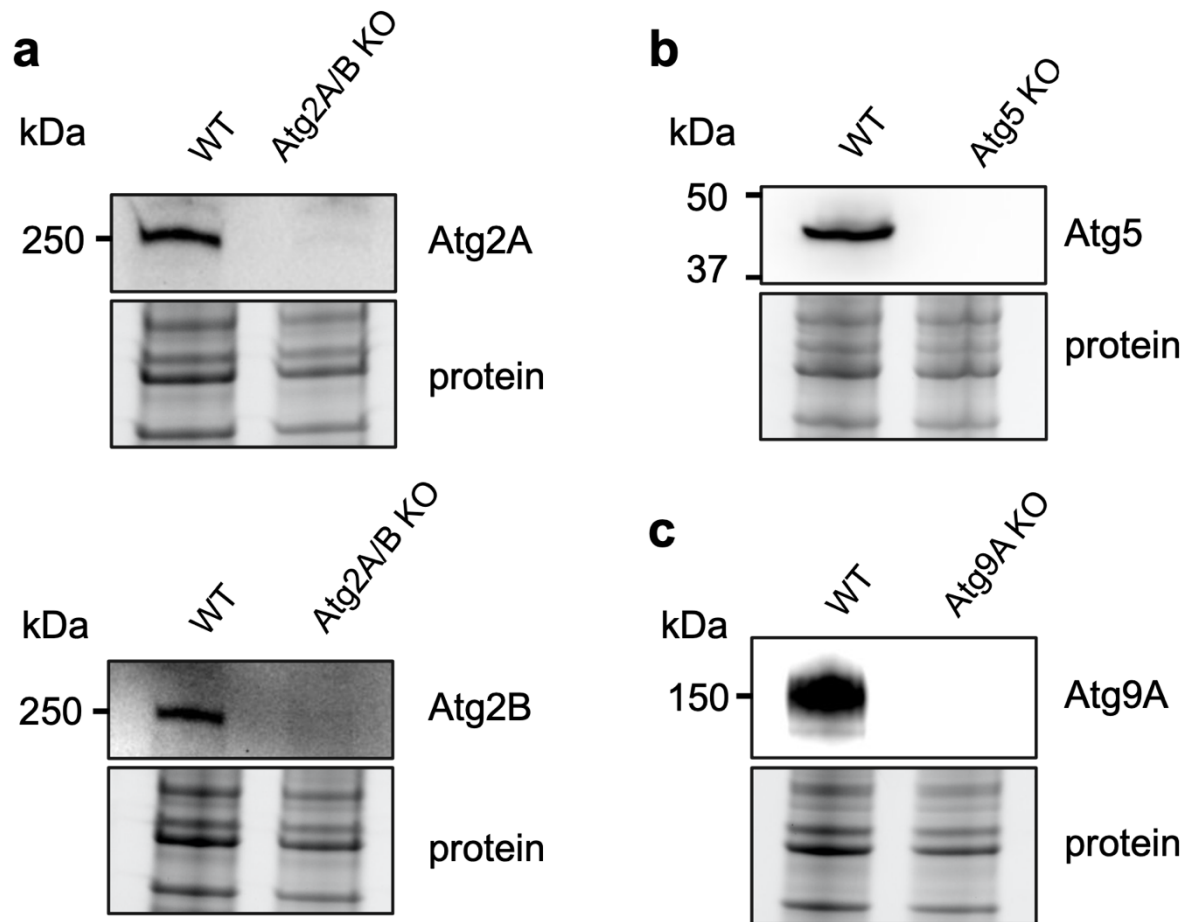
1126
1127
1128
1129
1130
1131 **Supplementary Figure 8. Characterization of Atg KO U2OS cells. a-c** Western blot
1132 characterization of U2OS Atg KO cell lines. **a** Atg2A/B KO cells; **b** Atg5 KO cells; **c** Atg9A
1133 KO cells. Whole-cell lysates were shown as a loading control.

1134
1135
1136
1137
1138
1139
1140
1141
1142
1143
1144
1145

1146
1147
1148
1149
1150
1151
1152
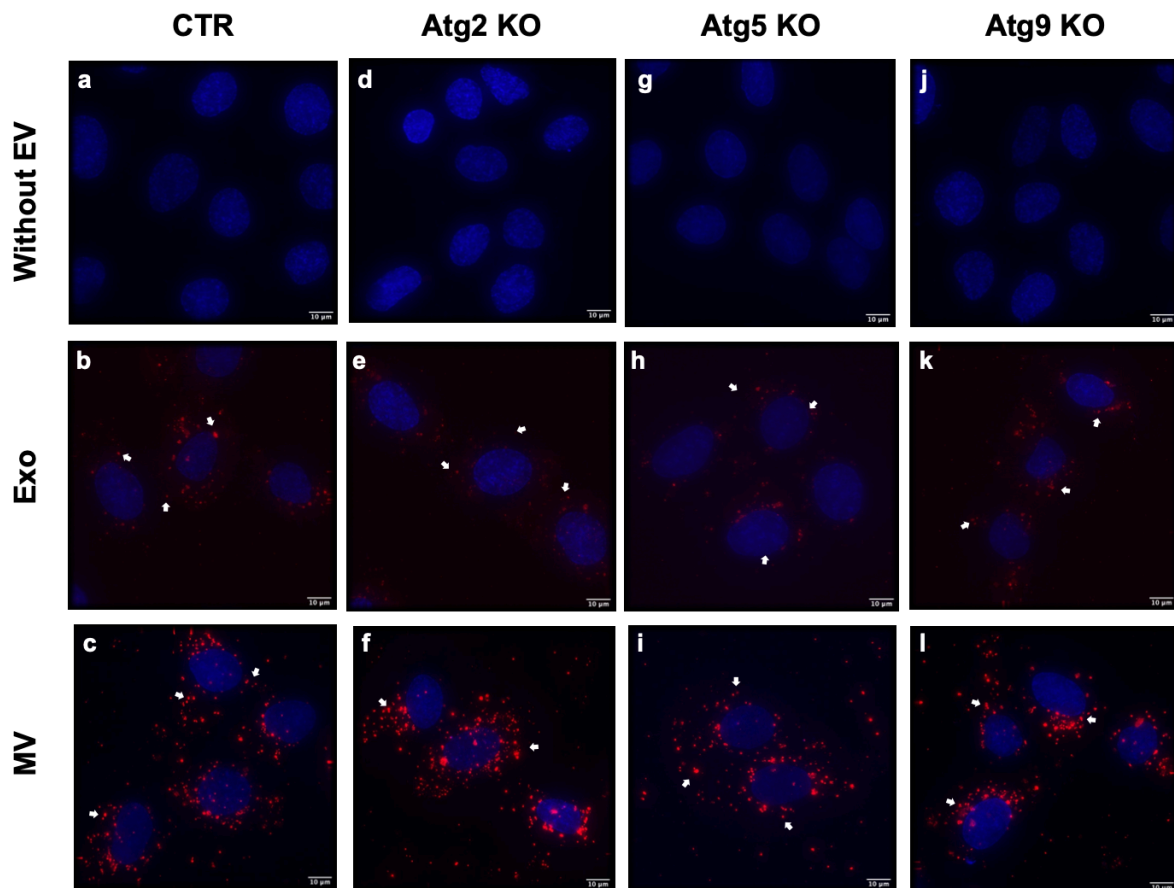
1153
1154
1155
1156

Supplementary Figure 9. Autophagy involvement in cellular uptake of exosomes- and MVs-PalmReNL. a-c Control cells; **d-f** Atg2 KO cells; **g-i** Atg5 KO cells; **j-l** Atg9 KO cells. Punctate signals of RFP (red) were merged with nuclei stained with Hoechst 33342 (blue). Scale bar, 10 μm. Arrows indicate RFP signals in PalmReNL-exosomes and -MVs taken up by the recipient U2OS cells.

1162
1163
1164
1165
1166

57

1167
1168
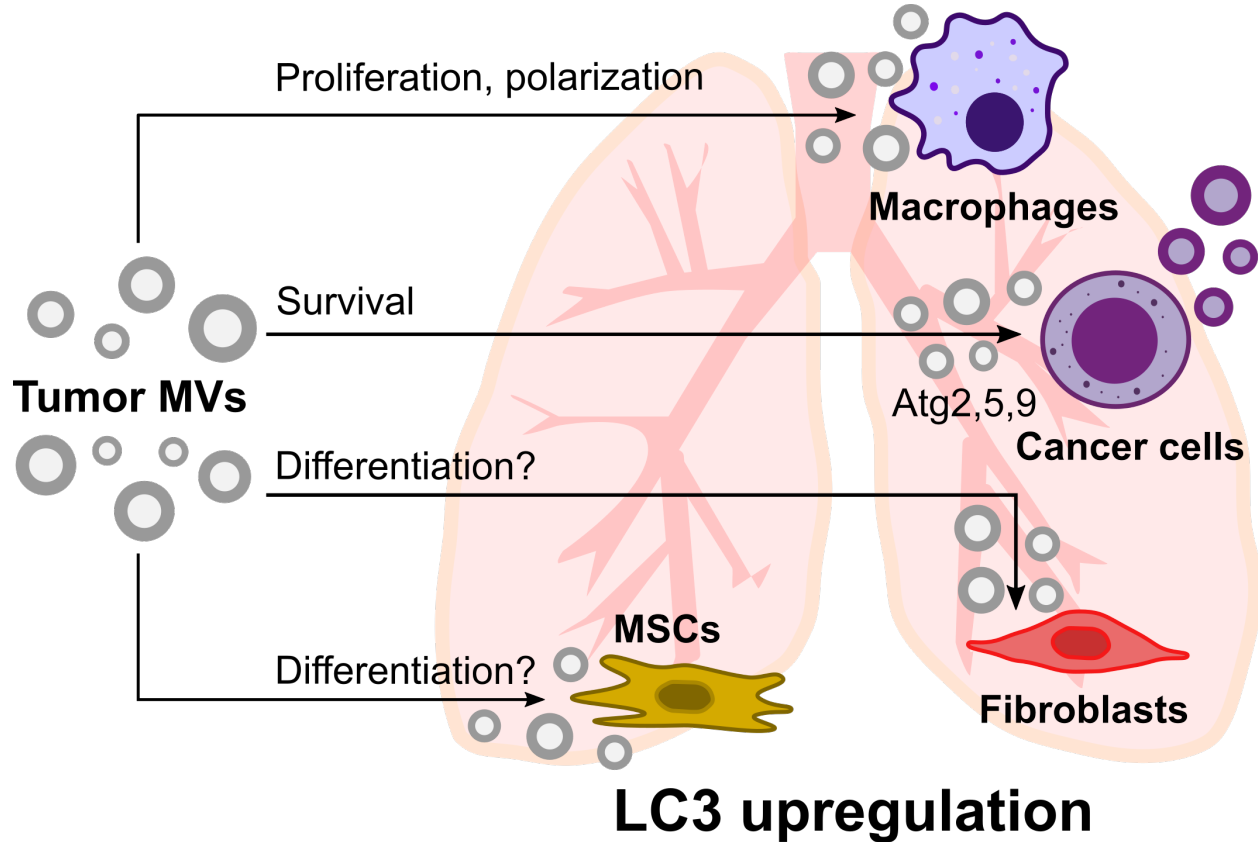
1169
1170
1171
1172
1173
1174
1175 **Supplementary Figure 10. Schematic representation of metastatic cancer cell**
1176 **survival in the lung promoted by MVs from primary tumors.** MVs released from
1177 primary tumors preferentially accumulate in the lung and affect various cell types,
1178 including macrophages, cancer cells, fibroblasts, and mesenchymal stromal cells (MSCs).
1179 Overall intercellular communication activates LC3 in the lung tissue and suppresses the
1180 anti-tumor response. Atg2, 5, and 9 proteins are directly and/or indirectly involved in
1181 metastatic cancer cells' EV uptake and release.
1182
1183